DaimlerChrysler Aerospace
Dornier
Dornier Satellitensysteme GmbH

MIRCAM

Mid-Infrared Wide Field Camera for NGST

&

MIRIFS

Mid-Infrared Integral Field Spectrograph for NGST

NGST – DSS – WHRP – 004

October 1, 1999

Work performed under ESA contract for the
"Study of Payload Suite and Telescope for NGST"
ESTEC/Contract no. 13111/98/NL/MS

Table of Content

0 INTRODUCTION 4

1 SCIENCE 6

1.1 SUMMARY 6
1.2 THE NASA DESIGN REFERENCE MISSION OVERVIEW 7
1.3 MID-IR SCIENCE FOR NGST 8
1.3.1 Mid-IR Studies of high redshift galaxies, expanding from ISOCAM surveys 8
1.3.2 Violent Star Formation and Nuclear Activity in Glaxies 11
1.3.3 Planetary Studies 13
1.3.4 Young Stellar Objects and the ISM 13
1.4 MID-IR INSTRUMENT TECHNICAL SPECIFICATIONS 15
1.4.1 Options for Mid-IR Spectroscopy on NGST 15
1.4.2 Mid-IR Camera Requirements 16
1.4.3 Mid-IR Integral Field Spectrograph Requirements 17
1.4.4 Instrument Operations 18

2 MIRCAM ENGINEERING 20

2.1 MIRCAM DESIGN CONCEPT 20
2.1.1 Instrument Overview 20
2.1.2 Optical Design of SW Channel 20
2.1.3 Optical Performance of SW Channel 22
2.1.4 Optical Design of LW Channel 24
2.1.5 Optical Performance of LW Channel 27
2.1.6 Photometric Instrument Performance 29
2.1.7 Opto-Mechanical Design 30
2.1.8 Budgets 32
2.1.9 Conclusions 33
2.2 CRITICAL AREAS AND RECOMMENDED DEVELOPMENT ACTIVITIES 34
2.2.1 Instrument Hardware Breakdown 34
2.2.2 Critical Areas and Technology Requirements 34
2.2.3 Recommended Follow-On Activities 35
2.2.4 Technology Development Roadmap 36
2.3 DEVELOPMENT PLANNING FOR PHASES B AND C/D 37
2.3.1 Work Breakdown Structure 37
2.3.2 Development Planning 38
2.3.3 Schedule 40

3 MIRIFS ENGINEERING 41

3.1 MIRIFS DESIGN CONCEPT 41
3.1.1 General Optical Design Considerations 41
3.1.2 Fore-Optics and Image Slicer Design Description 42
3.1.3 Short Wavelength Channel 45
3.1.4 Performance of the SW Channel 46
3.1.5 Long Wavelength Channel 48
3.1.6 Performance of the LW Channel 50
3.1.7 Instrument Photometric Performance 52
3.1.8 Opto-Mechanical Design 53
3.1.9 Budgets 56
3.1.10 Conclusions 56
3.2 CRITICAL AREAS AND RECOMMENDED DEVELOPMENT ACTIVITIES 57

3.2.1 Instrument Hardware Breakdown *57*
3.2.2 Critical Areas and Technology Requirements *57*
3.2.3 Recommended Follow-On Activities *58*
3.2.4 Technology Development Roadmap *59*
3.3 DEVELOPMENT PLANNING 59

4 REFERENCES 60

0 INTRODUCTION

As part of its Origins program, NASA is currently undertaking definition and feasibility studies of a Next Generation Space Telescope (NGST) to succeed the Hubble Space Telescope (HST) after 2005. NGST is foreseen to have an aperture of 8 meters and be optimized for near infrared wavelengths (0.6 - 10+ µms) in order to enable the exploration of the most remote high redshift universe.

NASA has invited ESA to extend their successful collaboration on HST to the NGST project, and a draft agreement concept is in place which aims at securing European participation in NGST at a similar level as on HST. ESA has undertaken a number of assessment studies which aimed at defining its potential instrument and spacecraft hardware contributions to the mission.

One of these ESA studies called “Study of Payload Suite and Telescope for NGST” (ref. /1/), has been conducted by Dornier Satellitensysteme GmbH (DSS), Ottobrunn, together with Alcatel Space (AS), Cannes, and a team of 16 European science institutes chaired by Laboratoire d’Astronomie Spatiale, Marseille, and UK Astronomy Technology Centre, Edinburgh. DSS took the responsibility for the overall study and the payload, AS for the telescope, and the science team was responsible for the instrument and telescope definition and requirements.

The **MIRCAM and MIRIFS** are two out of four instruments that were defined by the science team as potential NGST payload and were detailed by DSS.

For **MIRIFS** the optical system design and analysis was performed by UK Astronomy Technology Centre.

This document contains the instrument opto-mechanical design and analyses and the instrument specific development planning. Technical aspects that are common to all payloads studied by DSS (NIRCAM-FW, NIRCAM-FTS, MIRCAM, MIRIFS and IFMOS, which was studied under a separate contract) are described in a separate report, ref. /3/. These aspects include

- optical interface
- material selection, mechanisms
- thermal design and analysis
- electrical design, detectors, data processing
- common critical areas

Payload Study Team

ESA:

NGST study manager	J. Cornelisse
NGST study scientist	Dr. P. Jakobsen

Dornier Satellitensysteme:

Study mgmt., system engineering	W. Posselt
Optical engineering	Dr. W. Holota, P. de Zoeten
Mechanical engineering	D. Scheulen, H. Huether
Thermal engineering	A. Hauser
Electrical eng., data processing	W. Hupfer
Focal plane arrays	Dr. R. Buschner-Ueberreiter

Science Team:

Laboratoire d'Astronomie Spatiale	Dr. O. Le Fèvre
UK Astronomy Technology Centre	Dr. G. Wright

Chairing a consortium of the following institutes
Observatoire de Lyon
European Southern Observatory
Leiden Sterrewacht
University of Durham
University of Cambridge, Institute of Astronomy
Max-Planck-Institut für Extraterrestrische Physik
Observatoire de Haute Provence
Rutherford Appleton Laboratory
Max-Planck-Institut für Astronomie
Astrophysikalisches Institut Potsdam
Instituto de Astrofisica de Canaris
University of Leicester
Institut d'Astrophysique de Paris
Service d'Astronomique, CEA-Saclay

1 SCIENCE

1.1 Summary

The overall science goals of NGST will be met by a combination of instruments capable of carrying out observational programs in a wide range of wavelengths to address the key scientific issues as described in the NASA Design Reference Mission. Mid-IR instruments on NGST will be capable of carrying out aspects of many programs in the DRM. In addition the mid-IR is relatively unexplored at the spatial resolution and sensitivity NGST will be capable of, and so there is great potential for serendipitous science. We list below the key reasons why mid-IR capabilities covering the 5 - 30µm band will be important for the NGST:

- For wavelengths longer than 5µm NGST will surpass ground based 8m telescopes in sensitivity by 3 orders of magnitude, even for "worst case" NGST sensitivity.

- Even if the telescope performance is limited by scattered radiation from the sunshield, the "mid-IR compatible" telescope performance, it will be more sensitive than SIRTF and will have a critically important large spatial resolution advantage.

- Even although many ISO results are not yet published, there is already clear evidence that without observing the universe above 10µm, NGST would miss much of the star formation history. Other observations also indicate that even at high red-shifts most of the star-formation is dust enshrouded and the UV-optical tells only part of the story.

- Mid-IR lines provide truly unique diagnostics of star-formation, the interstellar medium and nearby galaxies.

- Mid-IR observations out to 30µm on NGST would:
  - Enable the identification the galaxies responsible for the IR background through their dust emission up to z = 3.8 for $10^{11}L_o$ galaxies and z = 8 for brighter ones.
  - Distinguish between dusty AGN and starbursts. This will be important in the future because at high redshifts only a few very bright galaxies dominate the IR background.

- Formation of stars and planetary systems occurs deep in molecular clouds, A_v > 100 , so can only be probed in the mid-IR at > 10µm

- Diffraction limited observations at 10µm will spatially resolve planet formation, holes in proto-planetary disks to 200pc. (SIRTF surveys will provide large samples)

- Unique information is provided by spectroscopy at 5-30µm, including all purely rotational H_2 lines, CH_4,CO_2, NH_3 H_2O. ISO has shown diagnostic value of mid-IR spectroscopy for solid material condensing during planet formation.

- ISO results show that most of the star-formation in interacting and merging galaxies is deeply embedded in dust. Mid-IR dust features and fine structure lines (at

>10µm) are essential to separate starburst and AGN as the power source in obscured galaxies. This study of physics of starbursts and AGN is central to our understanding of galaxy formation and evolution.

We briefly review the NASA design reference mission, and then discuss in more detail some of the science which mid-IR instruments on NGST would address. Instrument requirements are then derived.

1.2 The NASA Design Reference Mission Overview

The NASA Design Reference Mission has been defined with the goal to identify the most promising science NGST can do, and to help set the science requirements defining the instrument payload. A large fraction of the NGST mission is a core program, designed to understand the origin and evolution of galaxies, mapping dark matter, measuring cosmological parameters and study the physics of star formation. The DRM also includes a range of other studies which fall within the NASA Origins program. The goal is for the NGST to be capable of accomplishing the studies in the DRM in less than 3 years.

Table 1.2-1 presents the current list of DRM programs, as ranked by the NASA-ASWG.

Mid-IR camera and spectrograph capabilities are essential for 3 of the 7 core programs identified by the ASWG which are highlighted in this table.

A mid-IR camera which fully samples the diffraction limited images of NGST and has as wide a field as possible for survey work, will be capable of observations which will address the following DRM science areas : Formation and Evolution of Galaxies - Obscured Stars and AGN; Physics of Star Formation and proto stars; evolution of circumstellar disks; Evolution of organic matter in the ISM.

A mid-IR spectrograph with moderate spectral resolution (R >1000) with an integral field capability will be capable of observations which address the following DRM science areas : Formations and Evolution of Galaxies - Spectra; Formation and Evolution of Galaxies - Obscured Stars and AGN; Physics of Star Formation and protostars; evolution of circumstellar disks; Cool Field Brown Dwarfs, Properties of Kuiper belt objects, Evolution of organic matter in the ISM.

We discuss some of these mid-IR science goals in more detail in the following section, emphasizing particularly building on the ISO results, rather than the more general case.

Rank	Score	SDM	DRM Title
1	1.9	0.4	Form. & Evol. Galaxies- Imaging
2	2.9	0.4	Form. & Evol. Galaxies- Spectra
3	6.2	0.9	Mapping Dark Matter
4	6.8	0.8	Searching for the Reionization Epoch
5	7.3	0.9	Measuring Cosmological Parameters
6	7.8	1.0	Form. & Evol. Galaxies- Obscured Starform. &AGN
7	8.4	1.0	Physics of Star Formation: Protostars
8	10.5	1.0	The Age of the Oldest Stars
9	11.3	1.4	Detection of Jovian Planets
10	11.8	1.5	Evolution of Circumstellar Disks
11	12.0	1.5	Measuring the Rates of Supernovae
12	12.1	1.1	Origins of Substellar Mass Objects
13	12.2	1.2	Form. & Evol. Galaxies- Clusters
14	13.9	1.3	Form. & Evol. Galaxies near AGN
15	14.1	0.8	Cool Field Brown Dwarf Neighbors
16	14.6	1.1	Survey of Trans-Neptunian Objects
17	16.0	1.4	Properties of KBOs
18	16.8	1.0	Evolution of Organic Matter in ISM-Astrobiology
19	17.0	1.1	Microlensing in the Virgo Cluster
20	17.0	0.9	Ages and Chemistry of Halo Pops.
21	17.6	0.9	Cosmic Recycling in the ISM
22	18.5	0.8	IR Transients from GRBs and Hosts
23	18.7	0.9	IMF for Old Stellar Populations

Table 1.2-1: Ranked list of DRM programs (from NASA-ASWG). The core programs are shaded

1.3 Mid-IR Science for NGST

1.3.1 Mid-IR Studies of high redshift galaxies, expanding from ISOCAM surveys

Our knowledge of the mid-infrared (MIR) part of the spectral energy distribution of galaxies has greatly improved as a result of the ISO surveys. Most of the results of the ISO satellite have not yet been published, but we already can show that without observing the universe above 10 µm, NGST would miss much of the star formation history of our universe. In addition, while other instruments (FIRST and ALMA) will find very distant star forming galaxies, (despite the weak spatial resolution of FIRST and limitation of ALMA to distant galaxies for the estimate of the star formation rate), there will still remain the crucial question of the separation of the relative role of AGN versus starburst activity. ISOCAM mid-infrared spectra of galaxies have proved to be the best tool to distinguish a dusty AGN from a starburst (see below). This question will be the crucial one in the future, since we already know that going

to higher redshifts, a few very bright galaxies dominate the background and we know from IRAS ULIRGs that the most luminous galaxies are dominated by their AGN activity.

Several independent observations indicate strongly that most of the star formation taking place in early galaxies is dust enshrouded and optical-UV tells only a part of the story. The cosmic background due to the integrated flux from all galaxies over redshift is now detected over the wavelength 0.1µm to 1 mm. The power in the infrared part (dust emission) is about twice the power in the UV optical (G.Lagache 1998, PHD thesis, Hauser et. al. 1998, ApJ 508, 25, for COBE-DIRBE and Puget et al. 1996, A&A 308, L5, Guiderdoni B. et al. 1997, Nature 390, 257 for COBE-FIRAS). Locally the infrared component is only 40% of the UV-optical (Soifer & Neugebauer, 1991, AJ 101, 354). This ratio of 2 in the integrated power implies that at large z the infrared dominates strongly. The slope of the background, if it has to be filled with starburst type spectrum galaxies, implies that the far infrared production rate as a function of redshift goes up from z = 0 to z = 2 by a factor of 30 and stays constant up to at least z = 5. For IR galaxies below z = 1.5, the surveys carried out with ISOPHOT at 175 µm show a number counts slope (logN - logS) of 2.3. This strong cosmological evolution of far infrared sources is confirmed by deep surveys carried out with SCUBA at 450 and 850 µm (e.g. Smail et. al. 1997, ApJL 490, 5). ISOCAM detected typically 60 times fewer galaxies than HST, per unit area, but these few very bright infrared galaxies do produce at least one third of the integrated optical light. The 15 µm integrated background light above 50 µJy (ISOCAM deep surveys completeness limit) is about one third of the optical background measured in the HDF and one tenth of the DIRBE 140µm background. The galaxies making this 15µm background have been identified: their mean redshift is 0.7 and their total luminosity is close to $10^{12} L_{O}$., This means that, depending on model, between one third and all of the galaxies producing the 140 µm background have been identified by ISOCAM. In addition the HDF field results indicate a higher fraction of peculiar and interacting galaxies at high redshifts, and maps of nearby galaxies show that optically dark regions of interacting galaxies are subject to strong starburst phases only observable in the infrared (c.f. Mirabel et. a. 1998 A&A 333,L1). Taken together these results all indicate strongly that most of the star formation taking place in galaxies is dust enshrouded and that mid-IR observations beyond 10µm will be required for core NGST goals. Some key observations are described in the following.

The most important NGST observations beyond 10µm will be the identification of the galaxies making most of the star formation in the universe through their dust emission features (up to z = 3.8, for 10^{11} L_{O} galaxies, and up to z = 8, for brighter galaxies, through their 3.3 µm band). Figure 1.3-1 illustrates the detectability of such galaxies, based on the conservative assumption that their SED is similar to that of M82. Such observations require deep imaging surveys to identify galaxies, and low-moderate resolution spectroscopy. Extrapolating from the ISOCAM results indicates that at 25µm the 5σ/hour sensitivity limit of NGST corresponds to detection of 0.3 million galaxies per square degree with redshifts out to 3.

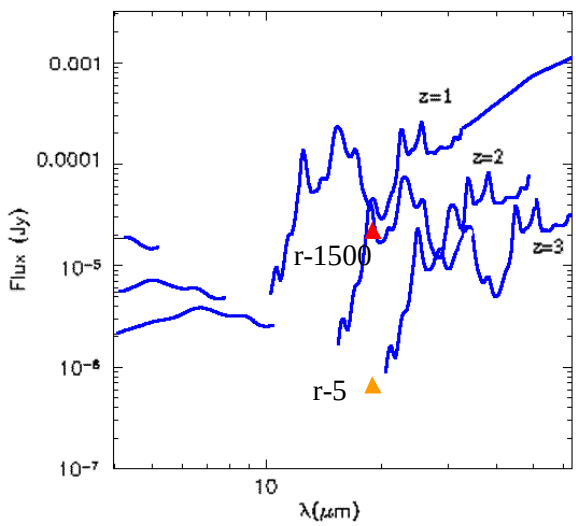

Figure 1.3-1: A 10^{12}L galaxy with an M82-like SED redshifted to z= 1, 2 and 3 is plotted. Its star formation rate would be close to 30 M .yr^{-1}, i.e. 5 times the SFR of M82, which is 5 times fainter. The SED of M82 was taken with the Circular Variable Filter (CVF) mode of ISOCAM on-board ISO, with a spectral resolution of R=35. The triangles mark the 5σ, 10^5 sec limiting sensitivities derived for our instrument concepts at 20μm.

The second most important NGST study, is to use red-shifted infrared lines to estimate the relative contribution of starbursts versus AGN in the energy source of these ultraluminous galaxies as a function of redshift using the ratio of aromatic bands intensity at 3.3, 6.2, 7.7 μm vs continuum (see Genzel et. al. 98). At lower spectral resolution, Laurent et. al. (in preparation) use ISO data to identify the signature of AGNs using only the shape of the continuum in the aromatic bands part of the SED. They show that the ratio of the continuum flux for $\lambda < 6\mu m$ to the mid-IR continuum is a good indicator of the relative importance of star-formation and AGN activity in providing the luminosity. Thus the photometric bands for a mid-IR camera on NGST should be designed to use such continuum features to track the evolution of AGNs as a function of galaxy evolution. Separation of starbursts and AGN is crucial since galaxies making most of the mid-infrared background below z = 1.5 (as measured by ISO) are a few bright galaxies with respect to optical-UV ones and may be dominated by an AGN activity that ALMA or FIRST will not distinguish from starburst activity.

One can conjecture that the infrared galaxies at z > 1 trace the merger phenomenon if merging of massive galaxies at these redshifts produce similar star bursts as those observed at low z. The infrared is thus likely to be the tracer of the history of merging in the process of building galaxies as we see them today. Among the galaxies detected with ISOCAM in the HDF, the fraction of galaxies with peculiar morphologies versus normal spirals increases with increasing redshift. Moreover,

integrated number counts become much higher than predicted from no evolution normalized to IRAS counts only below 1 mJy and very rapidly up to a factor 10 higher around 50 µJy. This rapid change in the slope of the number counts may reflect the dominant role of interactions above z = 0.4-0.5. Up to 25 - 30µm, NGST would probe the role of interactions up to z = 3.8 (taking the strong 6.2 µm aromatic band as a limit) and even z = 8, for brighter galaxies (including the weaker 3.3 µm aromatic band).

Determining star-formation history in different ways (UV dropouts, emission line surveys, dust emission etc.) shows that to get a quantitative measurement from observations that trace ONLY photospheric emission (at any wavelength) or nebular emission lines (which are always dominated by regions of lowest extinction) is difficult. (cf. Pettini et al. extinction estimates from Balmer lines). In contrast, a measurement of the dust emission at the short wavelength side of the Planck curve will give an estimate of total luminosity when a bolometric correction is applied. Detailed ISO observations of nearby galaxies indicate that this bolometric correction is uncertain by only a factor of 3 or less (depending on what rest wavelength you look at), which should be contrasted with the factor 10 uncertainty associated with measurements based on photospheric emission. Thus mid-IR measurements of the dust emission (λ_{rest} > 5µm) will be essential, at wavelengths longer than 10µm, if NGST is to make quantitative estimates of the star-formation history for galaxies at redshifts > 1.

1.3.2 Violent Star Formation and Nuclear Activity in Glaxies

Star formation in galaxies is not a continuous process. Many galaxies undergo bursts of intense star formation. During these periods, these galaxies evolve rapidly in stellar content, in gas content, in spectro-photometric properties, in luminosity, and often also in morphology. Starbursts are therefore an important mode of evolution of galaxies.

The most extreme starbursts are found in mergers of gas-rich galaxies, where the dissipative gas components quickly sink to the centre of the potential well, where an intense burst of star formation results. The ultraluminous infrared galaxies are a manifestation of this phenomenon, and approach quasar-like luminosities, which however almost totally emerges in the infrared regime. Based on these high luminosities, it has been suggested that powerful active nuclei are borne in the obscured cores of gas-rich mergers. Observational study of this important phenomenon requires the high angular resolution at infrared wavelengths that will be attained with NGST.

Starburst galaxies in the local universe are heavily enshrouded in dust, and therefore only accessible at infrared wavelengths. The most dramatic illustration of this effect is found in the nearby merging system NGC4038-4039 (the "Antennae"). Here HST has produced spectacular images of the optical emission in the remnant host galaxies, revealing numerous compact young star clusters. These sources represent young globular clusters formed as a result of the merger event. However, mid-infrared

images obtained with ISO show that most of the star formation takes place in an optically obscured region where the two disks interact directly. One spectacular star cluster in this regions accounts for more than 15% of the total luminosity, yet is optically totally invisible. High-resolution mid-infrared (10-30 µm) imaging will thus be needed to study the true, obscured, star formation properties of these rapidly evolving systems. Given the increased merger rate at higher redshifts, and the fundamental role that merging events play in the evolution of the galaxy population, understanding the physics of obscured starbursts is of central importance to our understanding of the evolution of the galaxy population as a whole. The availability of local "laboratories" that can be studied in detail makes this field an important science goal for NGST.

Spectroscopy in the 5 to 30 µm region is of fundamental importance in this study. This spectral range contains numerous forbidden fine-structure lines of abundant ions, that are excellent diagnostics of local kinetic temperatures and gas densities, and of the temperature of the exciting radiation field. In addition, this spectral range contains the lowest pure rotational transition on the H2 molecule. Multi-line spectra in this range can thus be used to disentangle starburst and active nucleus as power source of obscured galaxies (as has recently been demonstrated using ISO spectra of ultraluminous IRAS galaxies). For starburst galaxies, determining the high-mass cutoff of the Initial Mass Function in a spatially resolved fashion, will provide fundamental information on the immense compact star clusters in these obscured regions. Given that starbursts form an important mode of galaxy evolution, and that in particular the earlier stages of the build-up of the stellar population may be a violent, and mostly obscured event (after the first chemical enrichment and thus dust formation has taken place), the study of the physics of starbursts, targeting relatively local objects, is central to our understanding of the physics of galaxy formation and evolution.

Central to this project would be a diffraction-limited mid-infrared integral field spectrograph (5 to 30 µms) with a resolution of approximately 2000 and an instantaneous field of the order of 10" on a side, and it should be complemented by a diffraction-limited broad-band imager, equipped with a large variety of filters, in the same wavelength range. Core tasks for the spectrograph would be (i) full spectral imaging of a significant sample of luminous active galaxies of a variety of types and luminosities, including dusty starburst galaxies, starburst dwarfs, ultraluminous infrared galaxies, Seyferts and nearby QSOs, about 300 targets in total, to significant redshift (z = 1), in order to characterize the these populations, their physical nature and parameters, and their evolution towards earlier epochs, and (ii) a comprehensive study (with full spectral and spatial coverage of the active regions) of a smaller number (approximately 50) nearby starburst, ultraluminous and active galaxies, to be studied as local templates of more distant sources, and as Rosetta stones for understanding the astrophysics of violent activity in galaxies. For these galaxies mid-IR diagnostic lines can be observed on a spatial scale (~ 100pc) which is comparable to those of the optical HST studies of nearby Seyferts. A 3 kpc ring of star formation surrounding an AGN, such as that of the well known example NGC1068 could be

spatially resolved from the nucleus and detected by NGST for galaxies out to 100 kpc.

1.3.3 Planetary Studies

NGST will have the capability to do time-resolved and long-term studies of Solar System planets with high angular resolution and near IR capability. These detailed studies will build on the results of Space probe exploration. An example use is of methane on Jupiter and the outer planets, where it is the dominant gas absorber and has its transitions from the visible to the IR, giving access to information on different atmospheric depths. This line is in a difficult region for ground observations. Spectral resolution of R = 1000 - 10000 would be needed, and wavelengths to 8 µms would be useful. The large collecting area of NGST would be vital for Uranus and Neptune studies. Again, water observations and the molecular lines up to the extended 30 µm capability need an above atmosphere telescope, and the high spatial resolution of NGST means that the observations will resolve the disk. Pluto will be an important target, also resolved into10-20 ~ 0.01 arcsec pixels, because the atmosphere is expected to freeze.

The study of exoplanets has become a major topic in Astrophysics. The direct detection of exoplanets will allow their unambiguous identification and the measurement of their orbital motion. A highly-corrected NGST may be able to study Jupiter-like planets orbiting stars up to 10 pc away, and these NGST planetary searches will compliment those of IRSI or TPF where the interferometer will provide the extremely high spatial resolution necessary to find earth-like planets. A coronograph on NGST will be essential to conduct the observations.

1.3.4 Young Stellar Objects and the ISM

The formation of stars and their associated planetary systems are key questions for observational astronomy in the coming decades. These processes take place in the obscured interiors of molecular clouds, often behind more than 100 magnitudes of visual extinction. Therefore these regions cannot be probed using optical or even near-infrared techniques, except in more evolved cases where some of the dust has been cleared away. The early stages of the formation of stars and planetary systems are best observed in the mid-infrared.

The ISO satellite has revealed in the dust of large molecular clouds, where stars are forming, the ubiquitous presence of PAH compounds and of ices like H_2O, CH_4, CO_2, which are non detectable from ground-based observations. However, because of relatively poor spatial resolution, the clumpiness of dark clouds is known without the related chemistry of individual sources. To make significant progress in the study of the relation between the structure of gas and dust, the solid phase chemistry of molecular clouds throughout the history of star formation and the environment of new-born stars, high angular resolution near and mid-IR imaging and spectroscopy is required.

It is now known that circumstellar disks are a common by-product of star formation. These circumstellar disks become visible at 20 µm and longer wavelengths, since at 10µm the photosphere of the star still dominates. It is in these regions that planetary systems form, by coagulation of dust grains, followed by clearing away of the remaining gas and dust. High resolution observations at 20µm and longer wavelengths will spatially resolve this phenomenon. The forming planetary systems will clear out holes in the proto-planetary disks that may be resolved in images from NGST out to a distance of about 200pc. Previous missions such as SIRTF will deliver excellent samples for such observations from mid-infrared photometry at low spatial resolution.

Truly unique information is provided by spectroscopy in the 10-30µm region, where all the purely rotational H_2 lines will be available, as well as vibrational bands of important molecules such as CH_4, CO_2, NH_3 and H_2O, and solid-state features of crystalline material. The H_2 lines will be sensitive to molecular gas in the >50K temperature range, which is the expected temperature regime in these regions, and H_2 masses of 0.002 M_O (for T = 50K) will be readily detectable out to the rich star formation regions in Taurus and Auriga. This mass is 10 times lower than that of the minimum mass solar nebula! The power of solid-state spectroscopy in this region has dramatically been demonstrated by the ISO mission, which has revealed prominent spectral features due to crystalline silicates (in particular forsterite, Mg_2SiO_4) as well as olivines and crystalline FeO, in addition to prebiotic material such as PAHs. Remarkably, the inferred composition of the material closely resembles that of Comet Hale-Bopp in the solar system. Thus spatially resolved spectroscopy in this spectral region provides a unique diagnostic tool for probing the solid material condensing out of the proto-planetary nebulae during the onset of planet formation. Furthermore, current models of proto-planetary disks predict detectable vibrational bands of important gas-phase molecules such as CH_4, CO_2, NH_3 and H_2O, which are unique diagnostics for the formation of giant planets. These diagnostic tools are unique and the information they provide cannot be obtained in any other wavelength regime. They fit extremely well in the context of the NASA Origins program. Furthermore, there is no facility planned that will provide access to this spectral region at the required angular (0.3 arcsec for a representative sample of nearby stars) and spectral (R > 1000) resolution. Ground-based observations will not have the required sensitivity for continuum imaging (except a few exceptionally bright and uncharacteristic objects), and will provide only limited spectroscopic capability, with no access to crucial spectral diagnostics such as the lowest H_2 transition, molecular vibrational bands and crystalline features.

1.4 Mid-IR Instrument Technical Specifications

The mid-IR science goals call for both high resolution imaging with as wide a field as practicable, and for moderate resolution spectroscopy. It is clear that because of the cooling requirements as well as the smaller format arrays the total number of detector pixels will be much smaller in the mid-IR than in the near-IR. The mid-IR instrument design was kept as lightweight and simple as possible, with options for descoping should that be necessary. It is possible to conceive of instruments which combine imaging and spectroscopy with the same arrays used for either mode. This would of course require a mechanism for switching between the modes (e.g. flip mirrors, but other solutions are possible). For this preliminary phase we gave a high importance to simplicity, and so chose to have camera and spectrograph modules which are independent optically and use separate arrays. These were then treated separately as a mid-IR camera and a mid-IR spectrograph for the mechanical design. In addition both the camera and spectrograph have two channels and these were again designed as optically independent modules each with their own arrays, to keep the instruments very simple. As discussed in the following section we chose to study an integral field spectrograph for the spectroscopy. The range of modules (2 camera, 2 spectrograph) effectively explores the possibilities for the mid-IR for different numbers of arrays, and instruments could be de-scoped or simplified further by using fewer channels.

For the instruments' specification the upper wavelength limit was adjusted to 28 µm which forms the roll-off wavelength of the baseline Si:As detector arrays (ref. /3/).

1.4.1 Options for Mid-IR Spectroscopy on NGST

Although it is possible to combine a long slit and an image slicer type integral field unit in a single spectrograph this would involve the use of mechanisms. Given the requirements for simplicity, reliability and light weight it was decided that a single type of spectrograph should be chosen for study. This section explores the scientific drivers governing the choice between classical long-slit spectroscopy (LS) and integral field spectroscopy (IF) in the mid-IR spectral region on the NGST. In both LS and IF spectroscopy, one dimension of the detector chip is used as dispersion axis of the spectrum, i.e., there is no difference in spectral coverage. The other dimension of the detector chip is used for spatial information, but in LS spectroscopy this dimension corresponds to a narrow long strip of sky (the "slit"), i.e., spatial information is 1-dimensional, while in the IF spatial information is 2-dimensional. Principal science drivers considered in choosing IF over LS spectroscopy were:

Formation of Stars and Planets

This involves spectroscopy of circumstellar and protoplanetary disks in solid-state features and, vibrational lines of gas-phase molecules. Sizes of these circumstellar disks are typically several arcseconds, as shown by millimeter interferometry, but evolved cold debris disks could be larger as shown by recent SCUBA results. To 0th

order, circumstellar and protoplanetary disks might be expected to be axisymmetric systems. For a true axisymmetric system, it would be sufficient to have 1-dimensional spatial information, as long as there exists the possibility of rotating the slit to any position angle. This point is vitally important, not only for maximizing linear resolution across the disk under study by aligning the slit along the major axis, but also for addressing the dynamical state of the disk (e.g., Keplerian rotation). Most importantly however, the IF approach opens the way to finding deviations from axisymmetry in circumstellar and protoplanetary disks, e.g., concentrations at certain positions that could be due to the formation of giant protoplanets, orbital resonances etc., which are to be expected given current models. With a LS spectrograph this information can only be obtained by scanning the slit along the disk minor axis; however, this will be vastly less efficient than IF spectroscopy, It is thus concluded that for star and planet formation-related issues, IF mid-IR spectroscopy is strongly preferred over LS spectroscopy since it maximizes the scientific potential in this field of research and provides the most efficient method for studying disk structure.

Obscured Star Formation in Nearby Galaxies

This involves spectroscopy of bright forbidden fine-structure lines of ions and atoms, tracing various ionization stages in starburst regions and around active nuclei, and spectroscopy of H_2 rotational lines and PAHs. The power of this approach has been demonstrated by recent ISO work, but without any spatial resolution. The sizes of the regions involved are several arcseconds (up 15 arcseconds in nearby systems) but the smallest features such as "super-starclusters" are sub-arcsecond in size. There is generally no axisymmetry. These regions are mostly heavily disturbed and thus display no preferred axis, except in small circumnuclear starformation rings or circumnuclear tori around active nuclei. Given the lack of a preferred axis and the typical sizes of these regions, IF mid-IR spectroscopy is strongly preferred over 2D spectroscopy for these objects. Given the absence of a preferred axis in most targets, LS spectroscopy would be very inefficient compared to IF spectroscopy because study of excitation and kinematics over the full 2-D field is required.

Mid-IR Spectroscopy in High-z Galaxies

Since these very distant objects will probably not be spatially resolvable with NGST in the mid-IR, the reasons for preferring an IF spectrograph are based on the fact that it will minimize slit losses without compromising spectral resolution, and be unhindered by pointing errors. IF spectroscopy also means that for very faint marginally resolved sources it will be possible to bin spatial information to yield integrated properties without slit losses.

1.4.2 Mid-IR Camera Requirements

The goal is to observe simultaneously in two channels based on ISO survey results which show that the ratio of the continuum fluxes above and below 10µm will be a good discriminator of AGN and starburst activity in dusty high redshift galaxies.

As for the near-IR camera, the selection of pixel scale is a difficult choice requiring a balance between field and sampling of images at both the short and long wavelengths. An adjustable plate scale would mean extra mechanisms and so we chose instead to have different spatial sampling in each channel. Since the large aperture of NGST means that it will be capable of uniquely high spatial resolution compared to other space missions, including in the cosmologically important 5 - 7µm band which is not accessible from the ground, we chose to emphasize fully sampling the diffraction limited spot at the short wavelengths of each camera band.

Based on these decisions the requirements for the mid-IR camera were finalized to be as given in Table 1.4-1.

Instrument	**Item**	**Specification**
MIRCAM	Wavelength Range	5 - 28µm Two channels : 5 - 10µm, 10 - 28µm
	Field of View	2.5 x 2.5 arcmin
	Spatial sampling	0.075 arcsec / pixel (5 - 10µm) 0.15 arcsec / pixel (10 - 28µm)
	Sensitivity	Background limited
	Detector read out	non destructive reads

Table 1.4-1: MIRCAM High level technical specifications

1.4.3 Mid-IR Integral Field Spectrograph Requirements

For a compact simple instrument compromises were necessary. For a given spatial resolution and a fixed number of detector pixels there is a trade-off between the field of the integral field unit and the spectral resolution and coverage. As originally envisaged the requirements for this instrument specified a low spectral resolution mode (R= 200) with a larger (15 x 15 arcsec) integral field as well as a higher spectral resolution (R=2000) mode with a smaller 5 x 5 arcsec field. To achieve the two spectral resolutions in one instrument would have required inclusion of a grating or grism exchange mechanism (or a mechanism to switch the detectors from viewing one spectrograph to another). It was decided that it was most important to minimize the number of mechanisms in the instrument and hence to have only 1 spectral resolution. We chose moderate spectral resolution R = 1000 -2000 for the following reasons: (i) it is still just sufficiently high to facilitate the detection of lines in continuum sources, (ii) for 2k and 1k arrays a moderately wide spectral band width is still possible to maximize the observing efficiency when either observations of several lines are needed, or the redshift is uncertain. Given the limited number of pixels available in the mid-IR arrays, choosing higher spectral resolution would have meant using more orders (i.e. individual measurements) to cover the band. (iii) the performance could be close to background limited so that binning of spectral elements for lower resolution spectroscopy of faint sources is possible.

For spatial resolution a balance has to be made between sampling and field. We chose to specify two plate scales, one matched to the images at 5µm and the other at 10µm. This means that at the longer wavelengths the images will be over sampled and the data will have to be binned. Based on these considerations the performance requirements for the mid-IR integral field spectrograph became as shown in Table 1.4-2.

Instrument	**Item**	**Specification**
MIRIFS	Wavelength Range	5 - 28µm two channels: 5 - 10µm, 10 - 28µm
	Field of View 5-10µm Field of View 10-30µm	5.4 x 8.5 arcsec² 6 x 10 arcsec^2
	Spatial sampling	0.15 arcsec / pixel (5 - 10µm) 0.3 arcsec / pixel (10 - 28µm)
	Spectral Resolution	R > 1000
	Detector Readout	Non destructive reads
	Sensitivity	Background limited

Table 1.4-2: MIRIFS high level technical specifications

1.4.4 Instrument Operations

The **Mid-IR Integral Field Spectrograph** shall have the following modes of operation:

Single Channel Spectroscopy

Spectra will be obtained in one of the bands 5 - 10µm or 10 - 15µm, or 15 - 20µm, or 20 - 28µm. Repeated exposures will be summed to improve signal to noise. The telescope may be pointed to several contiguous areas to map a larger area, with spectra obtained at each position.

For some programs it may be necessary to move the telescope pointing so that the IFU looks at the source and then at a nearby "blank sky" position, to improve the background subtraction for sources which are larger than the field of view. The two observations are subtracted. (note that "classical IR chopping" modes will not be needed, due to the low NGST background).

Dual Channel Spectroscopy

This is as for single channel spectroscopy, except that the short wavelength and long wavelength channels will be used simultaneously. Thus spectra will be obtained for 5 - 10µm and one of 10 - 15µm, 15 - 20µm, or 20 - 28µm.

Flat Field Calibrations

These will be obtained from observations of a continuum source of known spectral type.

Photometric Calibrations

These will be obtained from observations of sources of known magnitude.

Wavelength Calibration

Confirmation of the wavelength calibration will be obtained from observations of a source of known unresolved emission lines. Since the grating is fixed, for the long wavelength channel calibration in one order only will be needed.

The **Mid-IR Camera** will have the following modes of operation :

Simple Imaging - Single Channel

In this mode a broad or narrow band filter is selected for either the short wavelength or the long wavelength channel and data are obtained with it. Repeated observations will be used to achieve the desired signal to noise. Jittering and "drizzling" techniques may be used to ensure the best spatial resolution, and remove bad pixels.

Two Channel Imaging and Surveys

In this mode a broad or narrow band filter will be selected for each channel and data obtained simultaneously for both. Repeated observations will be summed to achieve the desired S/N. Jittering and "drizzling" techniques may be used to ensure the best spatial resolution, and remove the effects of bad pixels. The telescope may be stepped through several positions with data taken at each position in order to map a larger area than the field of view for surveys or very extended sources.

Flat Field Calibrations

The flat field will be determined from the median of a jittered set of sky observations taken with the appropriate filter selected.

Photometric Calibrations

These calibrations will be determined from observations of stars of known magnitude.

2 MIRCAM ENGINEERING

Note: details on mechanical, thermal and electrical design can be found in ref. /3/.

2.1 MIRCAM Design Concept

2.1.1 Instrument Overview

In order to achieve the required simultaneous observations of two bands the MIRCAM is set up of two separate cameras:

- MIRCAM-SW - for the short wavelength range (5 to 10 µm)
- MIRCAM-LW - for the long wavelength range (10 to 28 µm)

The wavelengths for the two cameras MIRCAM-SW and MIRCAM-LW are split by a dichroic beam-splitter which is oriented under 45° with respect to the incoming beam. The dichroic beam-splitter transmits the short wavelengths (5 to 10 µm) and reflects the long wavelengths (10 to 28 µm). Proposed substrate material is ZnSe.

Both cameras have the same optical design principle. They are relay optics with different reduction ratios, that image the telescope focal plane onto the detector array. The different reduction ratios adapt the required different spatial resolutions to the same detector pixel sizes (the same Si:As detector arrays are foreseen for both instruments, see ref. /3/).

2.1.2 Optical Design of SW Channel

The optical configuration of MIRCAM-SW is based on the requirements of Table 1.4-1 and shown in Figure 2.1-1. It is an all-reflective design with a telecentric entrance pupil and a reduction ratio of 1.5. Then, a field of 2.5 arcmin by 2.5 arcmin is imaged on a detector array of 2K x 2K pixels of 30 µm each.

Note: when the optical design was performed the standard detector pixel size was erroneously assumed to be 30 µm. The design can however easily be adapted to a pixel size of 27 µm if the magnification is changed from 1.5 to 1.7.

Optical Design Description

The optics is a 3 mirror system (M1, M2 and M3). The front focal plane of M1 is adjusted to the telescope focal plane, resulting in a quasi-parallel beam (divergence < 30 mrad) between M1 and M2. This is a suitable location for the filter wheel.

M1 images the telecentric entrance pupil on its back focal plane, where M2 is located. In this way, the physical shape of M2 defines the aperture stop of the camera. M2 and M3 re-image the telescope focal plane onto the detector. The M1 surface is conical decentered and the two others are spherical decentered. The conic design is not critical with respect to manufacturing.

The detector array is cooled to a temperature < 10 K. The correct focusing on the image can be achieved by adjusting the detector array.

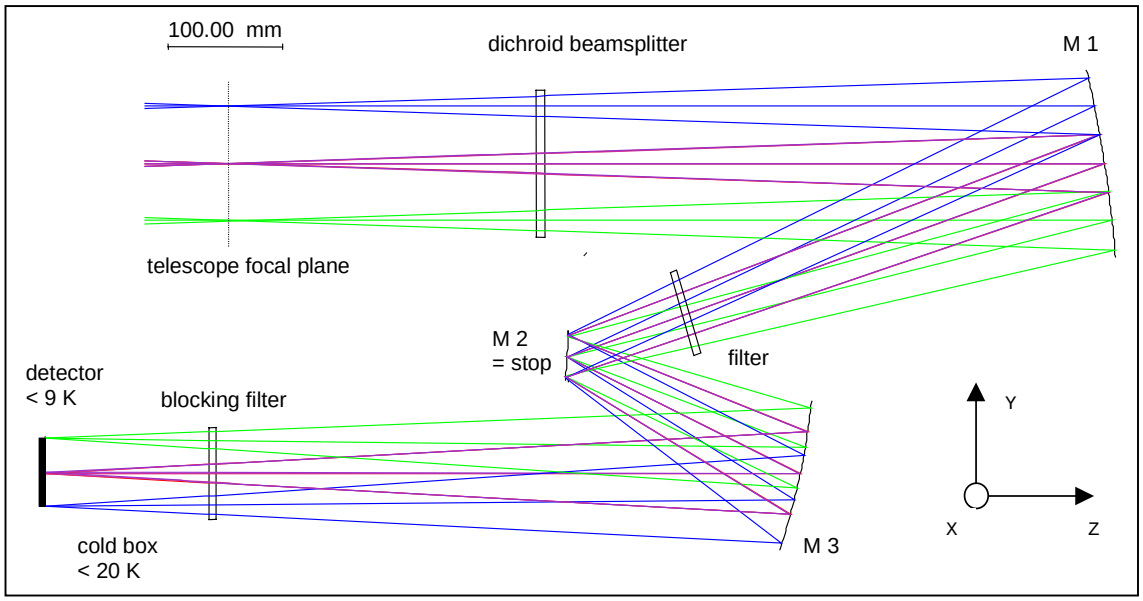

Figure 2.1-1: Optical configuration of MIRCAM-SW

Design parameters of MIRCAM-SW	
Parameter	**Value**
Wavelength range	5 to 10 µm
Reduction ratio	1.5
F-number at object side	16
Field (arcmin)	2.5‘ x 2.5‘
Detector array	2K x 2K
Pixel size	30 µm (see note above)
IFOV	0.32 µrad (or 65 mas)
Entrance pupil	telecentric
Stop	at second convex mirror
Stop diameter	37 mm
Optical surfaces	2 spherical, 1 conical
Spectral Filters	Filter wheel with 6 broad band filters and one open position

Table 2.1-1: MIRCAM – SW design parameters

Filtering

The broad band filters are accommodated on a filter wheel, which is located in the parallel beam close to the pupil stop.

Blocking filters on one or two substrates in front of the detector array block the wavelengths below 5 µm and above 10 µm. In the present design, there is one filter under an angle of about 36° to avoid ghost images.

2.1.3 Optical Performance of SW Channel

Image Quality and MTF

The optics have been optimized including the dichroic beam-splitter and blocking filter. The optical performance of the camera is diffraction limited.

The wavefront errors and Strehl ratios are given in the Table 2.1-2 below.

Wavefront errors of MIRCAM - SW and Strehl ratios calculated for a wavelength of 5 µm.			
Relative field position (X, Y)		Wavefront rms	Strehl ratio
0	0	0.034	0.95
1	1	0.042	0.93
-1	1	0.050	0.90
1	-1	0.046	0.92
-1	-1	0.055	0.89

Table 2.1-2: MIRCAM – SW wavefront errors and Strehl ratios

The MTF as a function of frequency is given in Figure 2.1-2. The MTF as a function of defocusing (through-focus MTF) for a spatial frequency of 6 cycles/mm is given in Figure 2.1-3. A defocusing of 0.25 mm gives a maximum decrease in MTF of about 7%.

Figure 2.1-4 gives the spot diagrams of the images at the detector. Figure 2.1-5 shows the lateral geometric and chromatic aberrations. In this figure it is also seen, that the chromatic aberrations due to dichroic beam-splitter and blocking filter are well compensated, so that the curves for the different wavelengths overlap.

The field angles are expressed in relative coordinates w.r.t. the maximum field angles.

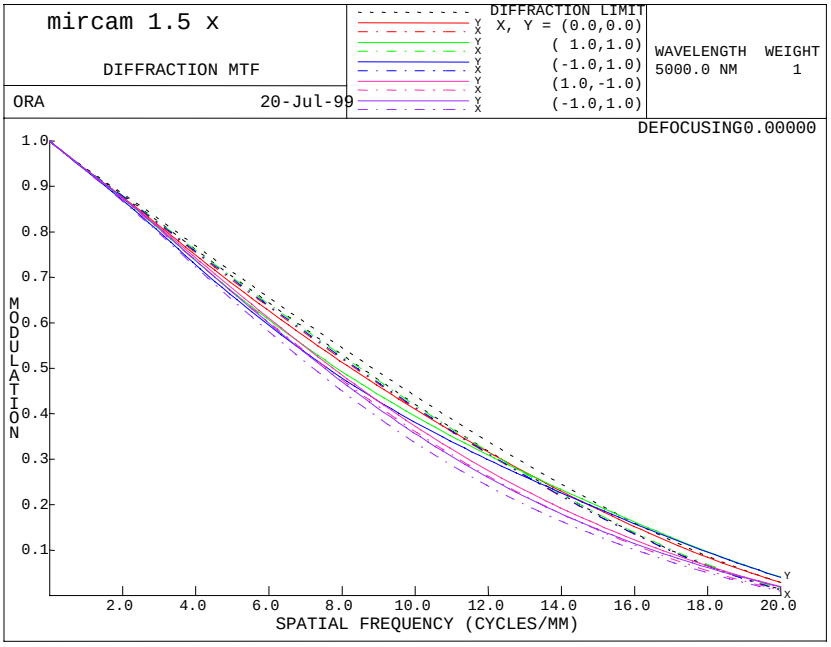

Figure 2.1-2: MIRCAM-SW: MTF as a function of spatial frequency calculated in center and corners of the field.

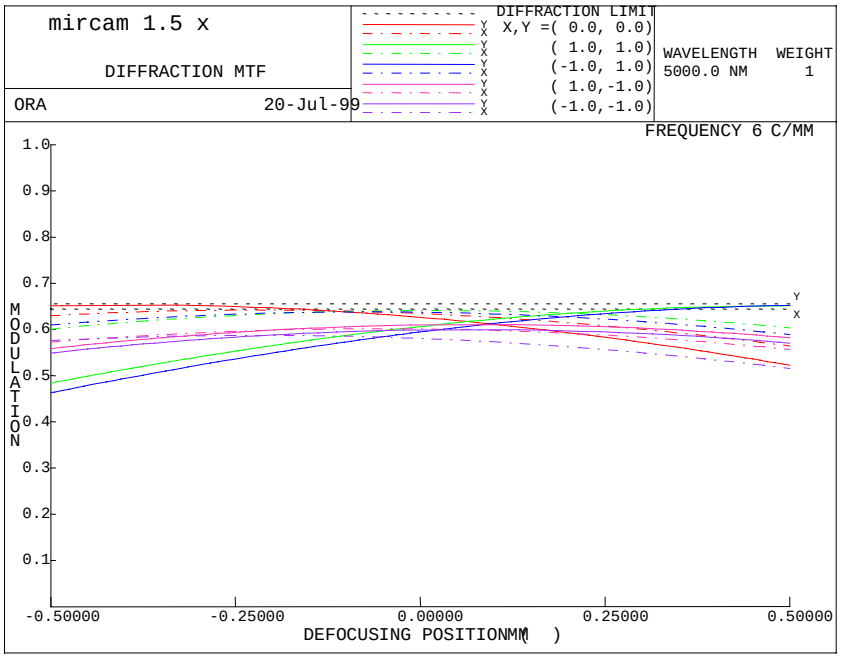

Figure 2.1-3: MIRCAM-SW: Through-focus MTF calculated in center and corners of the field for a frequency of 6 cycles/mm.

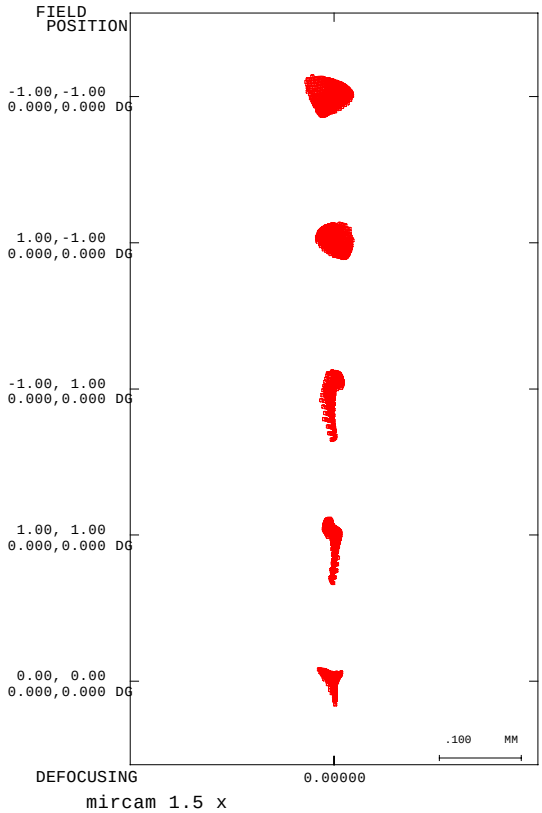

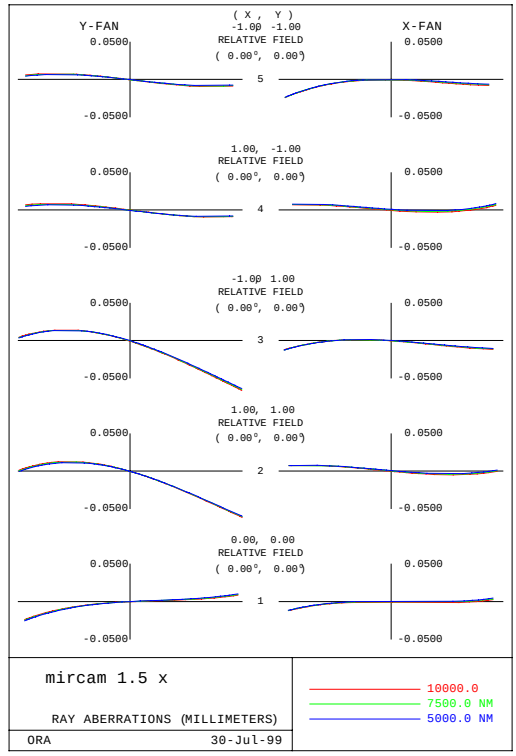

Figure 2.1-4 (left): MIRCAM-SW: spot images at detector in center and corners of the field for 10 µm wavelength.

Figure 2.1-5 (right): MIRCAM-SW: lateral (chromatic) aberrations at detector in center and corners of the field.

2.1.4 *Optical Design of LW Channel*

The optical configuration of MIRCAM-LW is shown in Figure 2.1-6. It is an all-reflective design with a telecentric entrance pupil and a reduction ratio of 3. Then, a field of 2.5 arcmin by 2.5 arcmin is imaged on a detector array of 1K x 1K pixels of 30 µm each.

Note: when the optical design was performed the standard detector pixel size was erroneously assumed to be 30 µm. The design can however easily be adapted to a pixel size of 27 µm if the magnification is changed from 3.0 to 3.3.

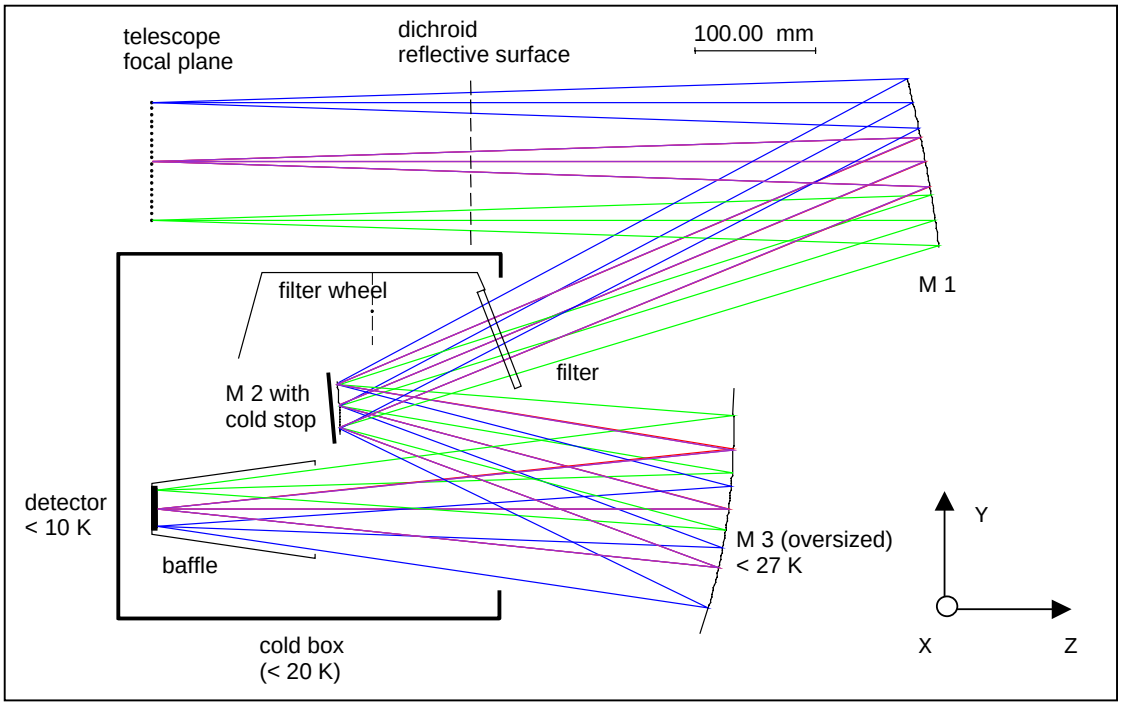

Figure 2.1-6: Optical configuration of MIRCAM-LW

Design parameters of MIRCAM-LW	
Parameter	**Value**
Wavelength range	10 to 28 µm
Reduction ratio	3
F-number at object side	16
Field (arcmin)	2.5‘ x 2.5‘
Detector array	1K x 1K
Pixel size	30 µm (see note above)
IFOV	0.63 µrad (or 130 mas)
Entrance pupil	telecentric
Stop	at second convex mirror
Stop diameter	38 mm
Optical surfaces	3 conical
Spectral Filters	Filter wheel with 8 broad band filters in parallel beam with one open position

Table 2.1-3: MIRCAM – LW design parameters

Optical Design Description

The optics is a similar system as the SW design with 3 mirrors (M1, M2 and M3). The front focal plane of M1 is adjusted to the telescope focal plane, resulting in a quasi-parallel beam (divergence < 30 mrad) between M1 and M2. This is a suitable location for the filter wheel.

M1 images the telecentric entrance pupil on its back focal plane, where M2 is located. In this way, the physical shape of M2 defines the aperture stop of the camera. M2 and M3 re-image the telescope focal plane onto the detector. All three mirror surfaces are conical decentered. The conical designs are not critical with respect to manufacturing.

The detector array is cooled to a temperature < 10 K. The correct image focus can be achieved by adjusting the detector array.

Thermal Design Description

In the long wavelength range above 10 µm, background radiation from the sun-shield and instrument thermal self-emission will be main contributors to the photon noise. The chosen configuration of the optical system allows measures to minimize these effects. All optical elements from the detector array up to and including the filters will have to be colder than the rest of the instrument. The thermal design is schematically shown in Figure 2.1-6.

The following measures to reduce the photon background are taken, and require thermal coupling to a low temperature cooler:

- all the imaging optics, including the filter wheel but except for the large third mirror, are located in a cold box and shall be kept at a temperature < 24 K.
- M3 is oversized, so that no radiation from behind the mirror is seen by the detector. This mirror should be at a temperature below 27 K.
- M2 acts as the cold stop. Behind this mirror, there is a cold black plate with an emissivity > 0.95. The plate temperature should be below 22 K.
- all mirrors shall have a reflectivity > 0.99 to keep the thermal self-emission low. In addition, they shall be very smooth (BRDF < $5 \cdot 10^{-4}$ sr^{-1} at 1° at a wavelength of 10.6 µm with a slope < -2.0) to keep the scattered radiation to a minimum.
- a baffle with a temperature below 20 K is designed such, that the detector does not see radiation from outside the cold box. If needed, extra baffles (not drawn) will avoid, that radiation from outside the cold box can only reach the detector after multiple reflections on black cold walls.

2.1.5 *Optical Performance of LW Channel*

Image Quality and MTF

The optical performance of the camera is diffraction limited. The wavefront errors and Strehl ratios are given in Table 2.1-4 below:

Wavefront errors of MIRCAM - LW and Strehl ratios calculated for a wavelength of 10 µm.			
Relative field position (X, Y)		Wavefront rms	Strehl ratio
0	0	0.003	1.00
1	1	0.010	0.99
-1	1	0.010	0.99
1	-1	0.006	0.99
-1	-1	0.006	0.99

Table 2.1-4: MIRCAM –LW wavefront errors and Strehl ratios

The MTF as a function of frequency is given in Figure 2.1-7. The MTF as a function of defocusing (through-focus MTF) for a spatial frequency of 6 cycles/mm is given in Figure 2.1-8. A defocusing of 0.25 mm results in a maximum decrease in MTF of about 7 %.

Figure 2.1-9 gives the spot diagrams of the images at the detector in the center and the corners of the field. Figure 2.1-10 shows the lateral geometric aberrations.

The field angles are expressed in relative coordinates w.r.t. the maximum field angles.

The wavefront quality of MIRCAM-LW is actually better than that of MIRCAM-SW, because in MIRCAM-LW three conical mirrors are used, while in MIRCAM-SW only one conical and two spherical mirrors are used.

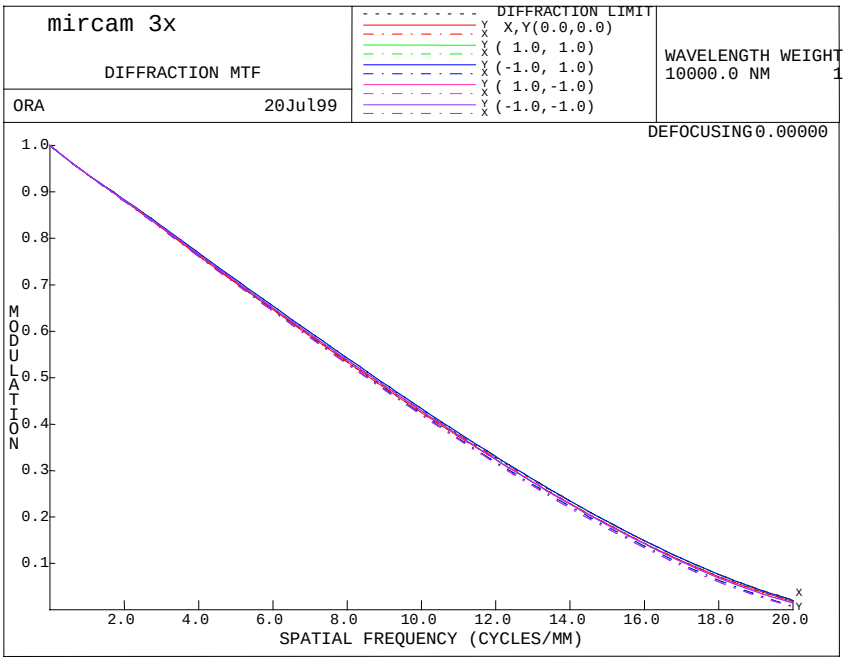

Figure 2.1-7: MIRCAM-LW: MTF as a function of spatial frequency calculated in center and corners of the field.

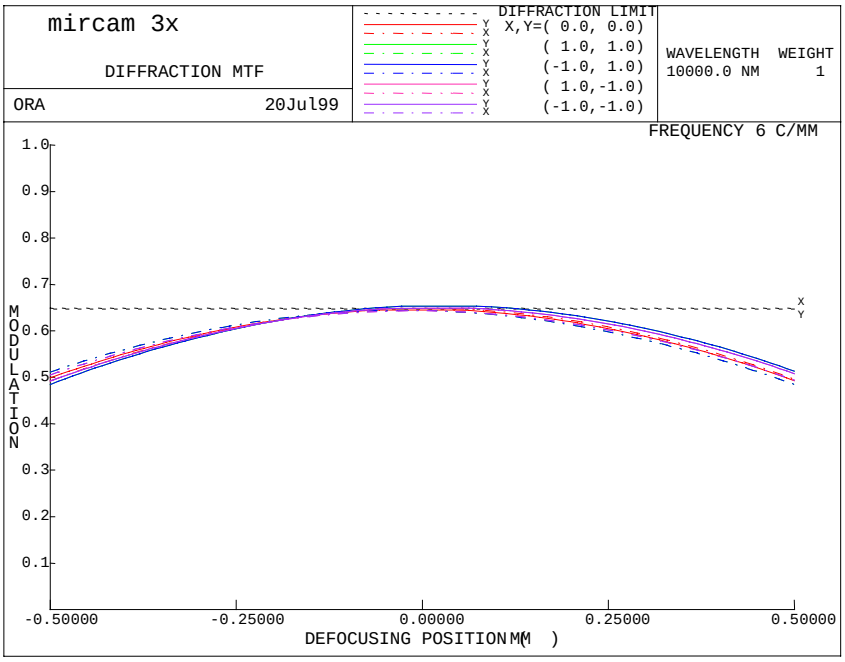

Figure 2.1-8: MIRCAM-LW: Through-focus MTF calculated in center and corners of the field for a frequency of 6 cycles/mm.

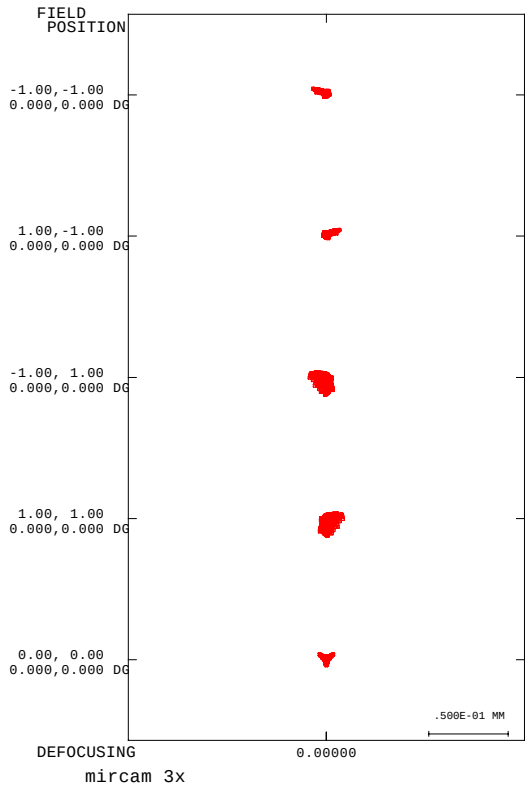

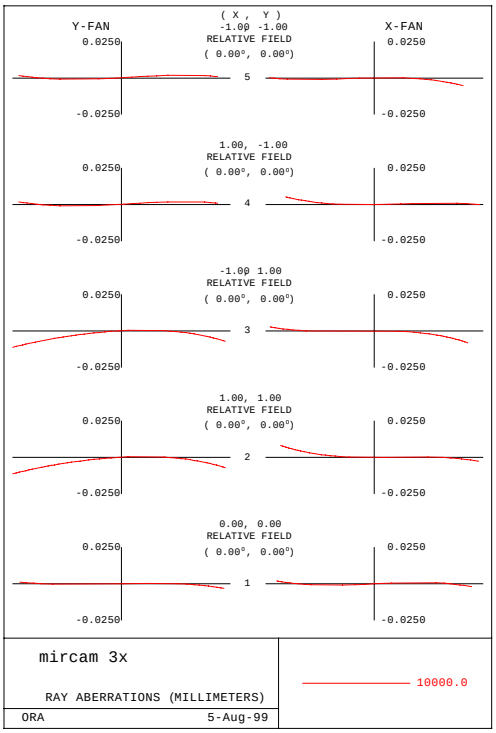

Figure 2.1-9 (left): MIRCAM-LW. Spot images at detector in center and corners of the field.

Figure 2.1-10 (right): MIRCAM-LW. Lateral aberrations at detector in center and corners of the field.

2.1.6 Photometric Instrument Performance

A photometric performance model has been established to simulate the expected in-orbit instrument performance. The model includes all efficiencies from the telescope transmission up to the detector quantum efficiency. As photon background the following contributions have been considered

- zodiacal light (ref. /4/)
- emission from sunshield, scattered by telescope prime mirror (ref. /5/)
- emissions from warm optics in front of the filter
- emissions from cold optics and environment up to and including the filter

Figure 2.1-11 show the detectable flux [nJy] of point objects as a function of wavelength that can be resolved with broad band filters in the short and the long wavelength region with a SNR of 10 and for 10^5 sec observation time.

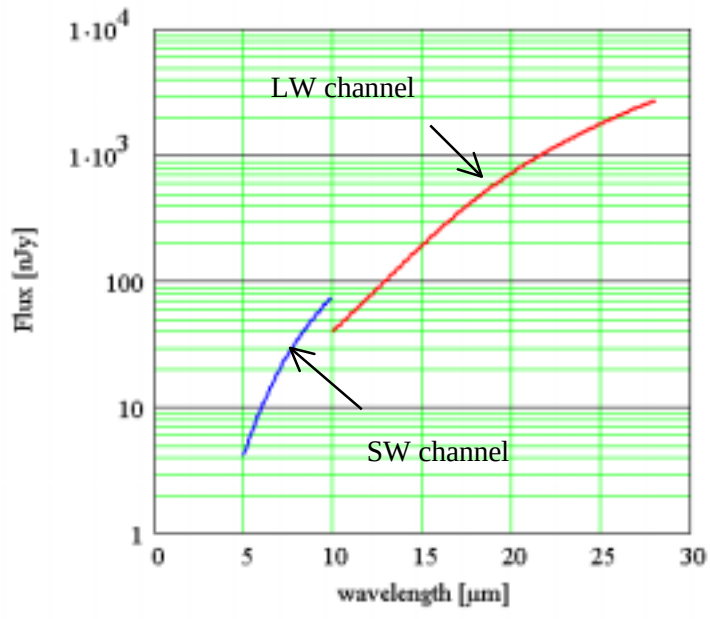

Figure 2.1-11: flux of point sources vs. wavelength that can be resolved in the short and long wavelength region with an SNR of 10 and an observation time of 10^5 sec

Discussion of Result

The performance is for all target magnitudes photon noise limited. Dominant noise sources are the zodiacal light and – much worse – the scattered light from the sunshield. If the surface quality of the telescope prime mirror cannot be improved considerably, then the scattered light contribution can only be reduced significantly by lowering the sunshield temperature from 90 K to about 70 K.

In case the ISIM is at < 35 K the emissions from the warm optics are negligible. The cold optics temperature of about 18 K has been selected such that this contribution will also be negligible. The detector and the readout noise are negligible for all targets (Fowler sampling has been assumed).

2.1.7 Opto-Mechanical Design

The baseline opto-mechanical designs are shown in Figure 2.1-12 to Figure 2.1-14.

The optical bench as primary structure consists of a light-weighted plate made of C/SiC material. The C/SiC brackets for the optical components are directly attached to the baseplate. The mirrors are connected to the brackets by an isostatic 3 point support. Flexible INVAR mounts are used as connection elements.

In Figure 2.1-13 the cold housing cover of the LW channel is removed to show the accommodation of the cold optical elements inside.

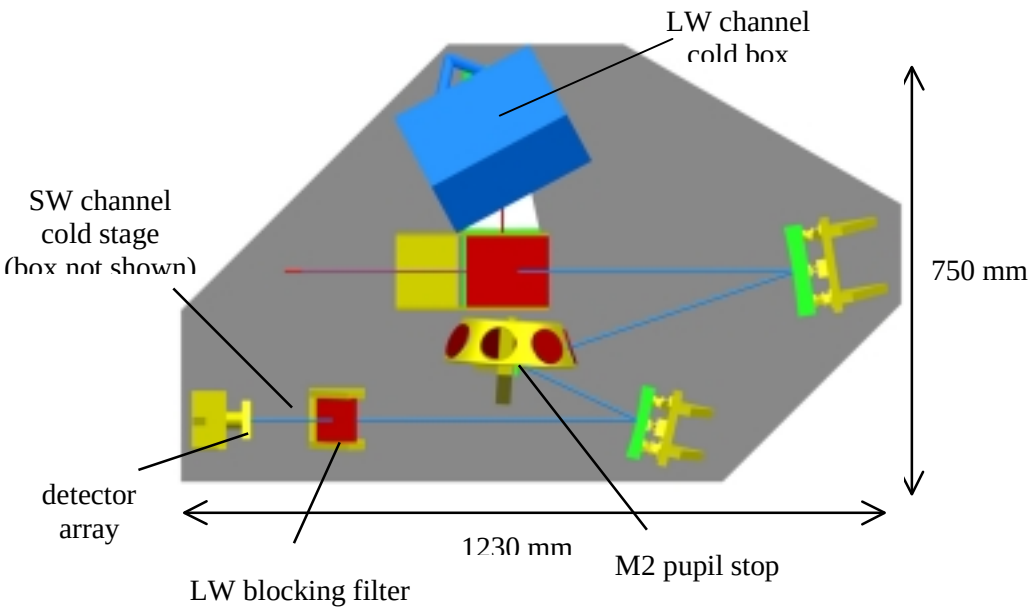

Figure 2.1-12: MIRCAM design: top view on the SW channel. The LW optical path is perpendicular to the image plane

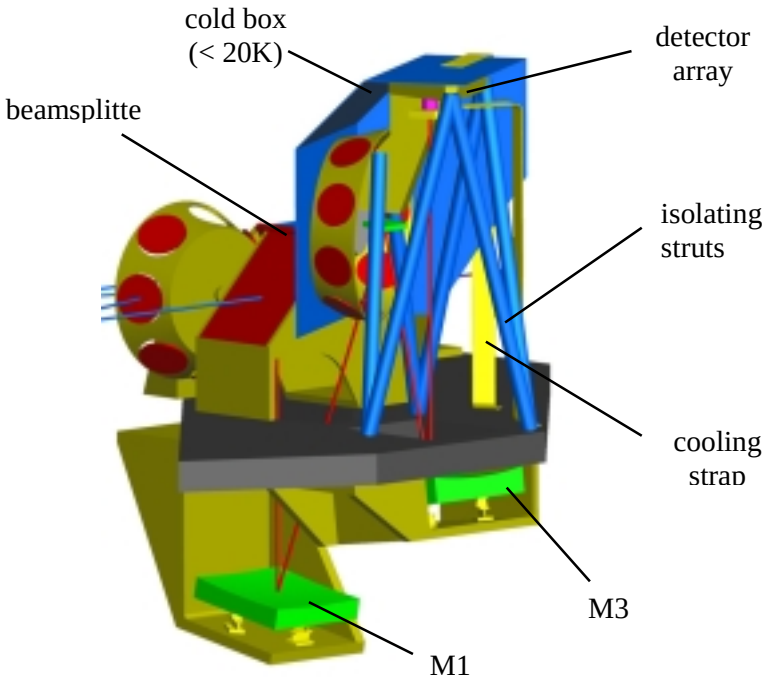

Figure 2.1-13: MIRCAM design: close view at the LW channel with the housing partially removed. Long CFRP bars provide good thermal isolation of the cold parts.

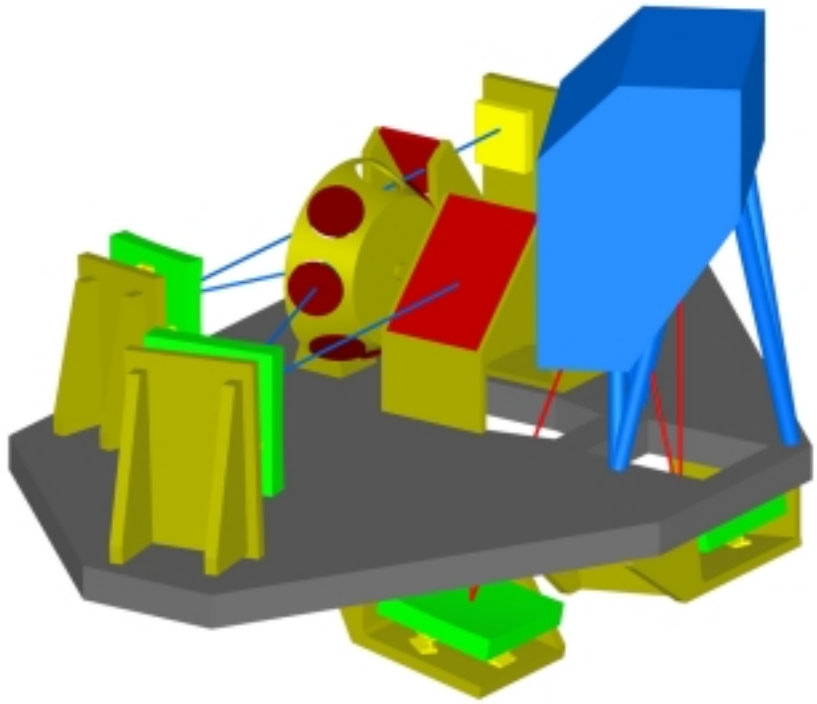

Figure 2.1-14: MIRCAM design: 3D view. SW channel on the left (blue rays), LW channel on the right (red rays). A large dichroic in the center (red) splits the beam.

2.1.8 Budgets

The overall dimensions of the MIR Camera are: 1.23 x 0.75 x 0.78 m^3

The estimated overall mass of the MIR Camera is 45 kg (Table 2.1-5).

	Mass [kg]
Primary structure	21
Brackets, mounts, filter wheels	6
Optical components	7
Thermal hardware	1
Miscellaneous (I/F brackets, harness, etc.)	10
Total	**45**

Table 2.1-5: MIRCAM mass budget

2.1.9 Conclusions

The presented Mid Infrared Camera design is very compact, taken into account the large field provided. The optical performance is very good over the whole field, and thus an optimization towards an even more compact design could be envisaged.

Summary of the design and performance features:

+ very good optical performance
+ compact overall design for the LW- and the SW-range
+ efficient cold stop in MIRCAM-LW located at the secondary mirror, that can easily be cooled
+ the thermal design guarantees a good reduction of instrument background radiation
+ filter wheel in parallel beam
- large dichroic beam-splitter

Possible improvements:

+ a design optimization to reduce the size by about 20% seems possible without measurable reduction in performance

The following work is recommended for the next study phase:

- filter definition and design
- investigation of expected optics defocusing (need of refocusing mechanisms)
- analysis of stray-light, thermal self-emission and ghost images (narcissus).

2.2 Critical Areas and Recommended Development Activities

2.2.1 Instrument Hardware Breakdown

Figure 2.2-1 shows the HW breakdown of the filter wheel camera. The shaded boxes provide an overview of potential critical subsystems or of subsystems containing critical elements as listed in chapter 2.2.2.

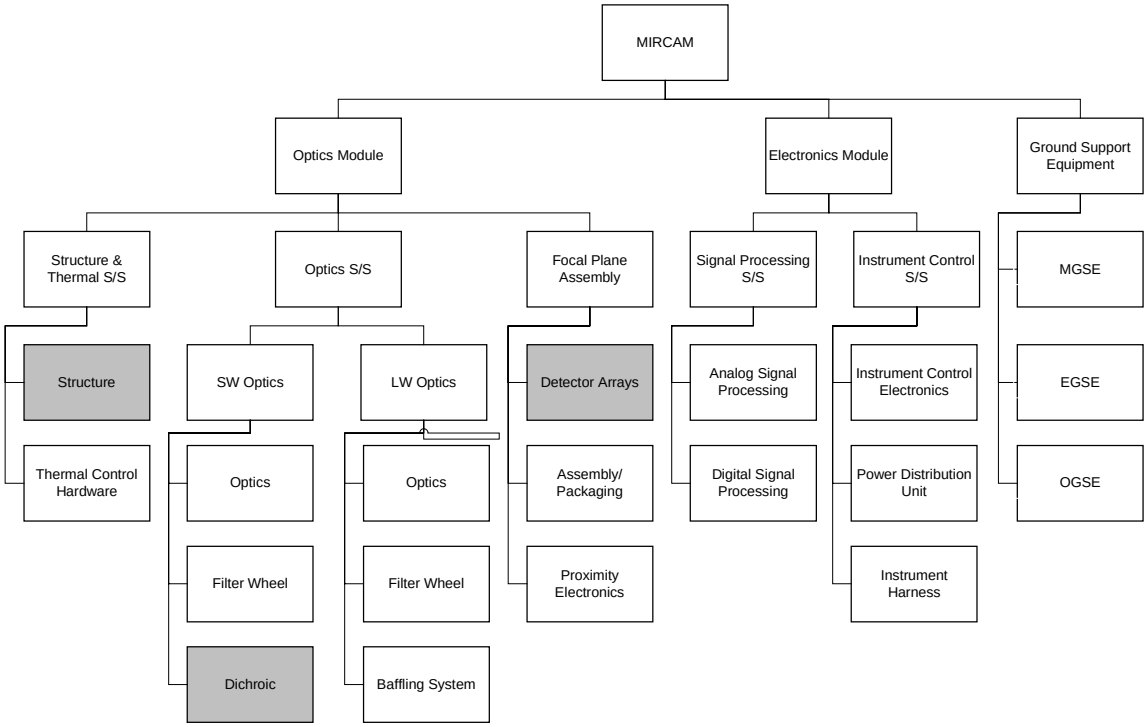

Figure 2.2-1: Instrument Hardware Breakdown; shaded areas indicate potential critical subsystems.

2.2.2 Critical Areas and Technology Requirements

Potential criticalities to be considered during the development of the instruments are

- items whose failing may affect the satellite performance or survival probability
- single point failures and non-redundant major elements
- items whose failing/degradation may affect the instrument performance
- items not previously space qualified
- items with exceptional process sensitivity and long lead items

The critical areas of the MIRCAM are mainly concerned with the last two items, i.e. subsystems which contain new technologies or technologies of expected long development duration. These technologies should be identified in an early stage of the project to allow definition of a dedicated technology development program in order to reduce the development risks of the project.

Critical Areas and Risks

In ref. /3/ a generic list of critical areas had been provided, which is valid for all instruments under consideration, like structure material or detector development. Instrument specific areas of potential criticality for MIRCAM are summarized in the following Table 2.2-1.

Subsystem	Critical area	Comments
dichroic beamsplitter	performance and mounting of large dichroic	spectral drifts during cool-down, differences in CTE

Table 2.2-1: Potential critical areas of MIRCAM

Technology Requirements

The dichroic will have a different CTE than the instrument structure, and its mounting should be demonstrated in an early stage of the project. The dichroic will need to be mounted in a way which avoids stress during cool-down and which will survive the launch loads.

Low temperature filter wheels have been built, qualified and flown for ISOPHOT, ref. /3/. It is therefore expected that this item can be managed within normal engineering work and does not require breadboarding activities (tbc).

2.2.3 Recommended Follow-On Activities

Technology Development Activities on Instrument Level

In order to minimize the development risks the following technology development activities are recommended.

- verification of C/SiC material for structural and optical components
- verification of dichroic performance and mounting technology

For each of these activities, the following technology development activities are proposed:

- critical review of existing technologies
- design and manufacturing of a representative unit
- verification of performance prior to and after environmental tests, at ambient and at operating conditions

The expected duration of the development activities is 15 months.

Technology Development Activities on System Level

There are other technology verification activities which are considered necessary, especially the developments of the detectors. Whether or not mechanisms for refocusing will become necessary can not yet be decided. But these technologies will be needed for other NGST hardware units as well and it is assumed that they will be developed on system level (under NASA contracts).

2.2.4 Technology Development Roadmap

The technology development roadmap for the major critical technologies is depicted in Figure 2.2-2 below.

The instrument specific hardware elements which are recommended for technology development are

- C/SiC material at cryogenic conditions
- filter wheel mechanisms and filter mounting

The system level hardware elements that are recommended for technology development are (corresponding developments activities are on-going)

- large and low noise detectors
- actuators/mechanisms for refocusing (tbc)

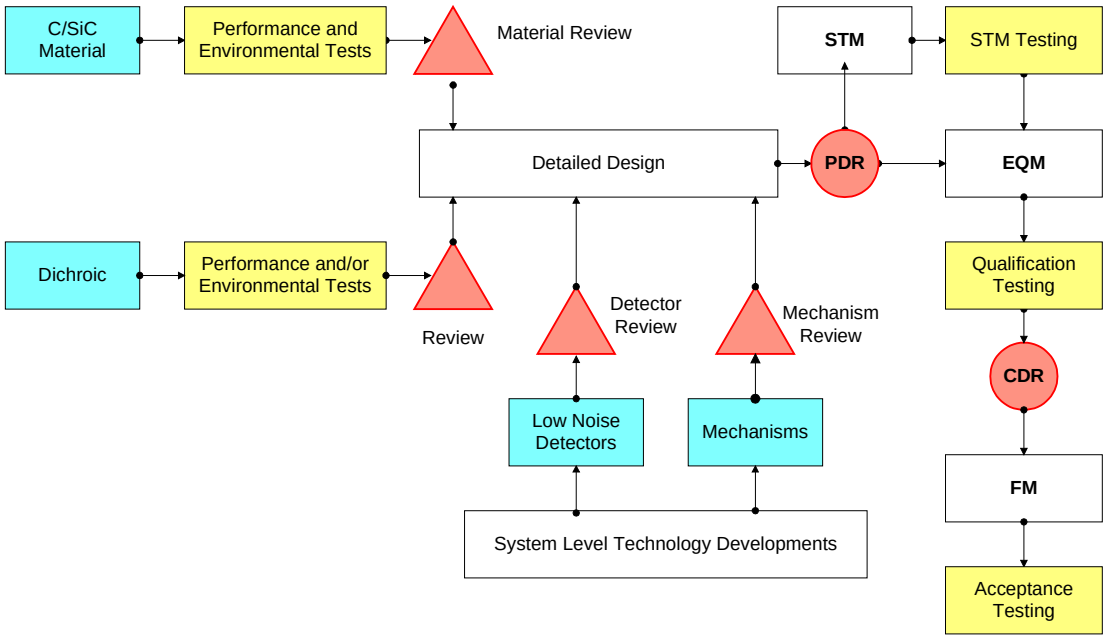

Figure 2.2-2: Technology Development Roadmap

2.3 Development Planning for Phases B and C/D

2.3.1 Work Breakdown Structure

The function oriented Work Breakdown Structure (WBS) is shown in Figure 2.3-1 below. The project is subdivided in management, product assurance, engineering, MAIT and procurement tasks. This WBS and the hardware breakdown shown in Figure 2.2-1 form the basis for the industrial cost estimate.

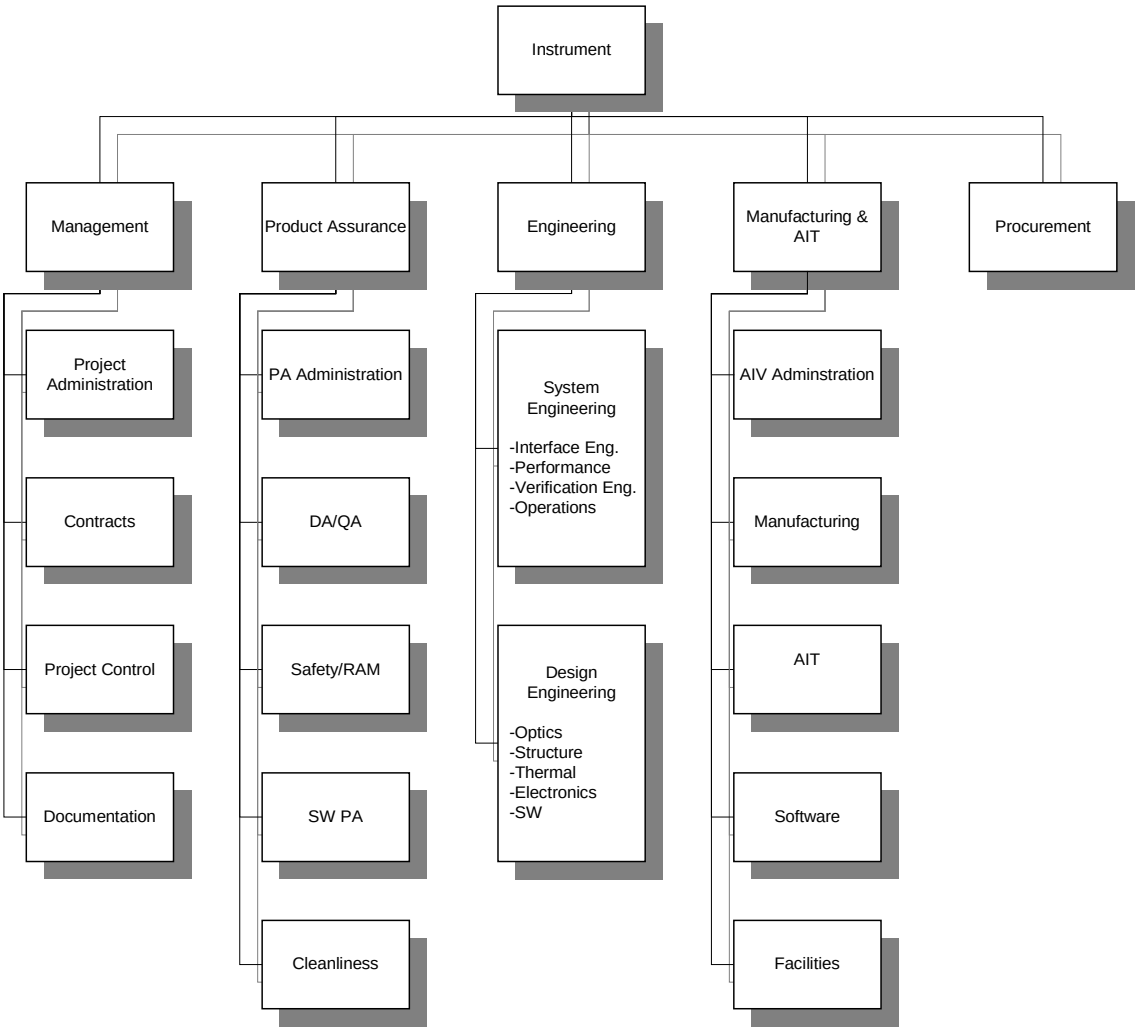

Figure 2.3-1: Function oriented Work Breakdown Structure

2.3.2 *Development Planning*

Two model philosophies have been considered for Phases B and C/D:

- **Standard Model Philosophy** (or standard development approach), according to a typical ESA space project and aiming for low risk
- **Alternative Model Philosophy** (or alternative development approach), trying to meet the NASA schedule

Standard Model Philosophy and Schedule

The standard philosophy is based on a typical (European) space project approach and shown in Figure 2.3-2. The development risk is minimized by building a set of prototypes and models: any design deficiencies identified on a lower level model can be eliminated on the subsequent higher level model. The sequential flow of models and associated learning steps will minimize potential risks for the flight model.

Besides technology breadboards and prototypes the following models are envisaged:

- Structural/Thermal Model (STM)
- Engineering Qualification Model (EQM)
- Flight Model (FM)
- Flight Spare

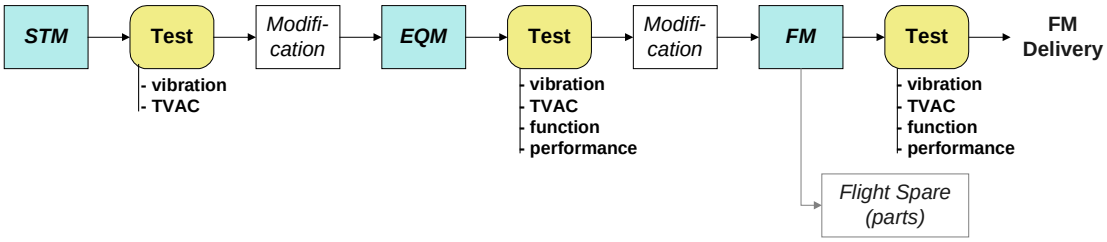

Figure 2.3-2: Standard Model Philosophy

The STM will be used to test the structural and thermal performance at low temperatures and after launch loads. Likely design modifications for the EQM will be derived. The STM will then be shipped to NASA for system level tests.

The EQM will be fully equipped and will undergo all performance and environmental tests on qualification levels. Design modifications for the FM will be derived, if necessary. The FM will be tested to acceptance levels only. The flight spare will consist of a set of instrument functional units and spare parts.

Drawback of this approach is the long development duration: the FM delivery will not be before end of 2007, see Figure 2.3-4. This delivery date is about 1.5 years later than scheduled by NASA.

Advantage of this approach is the identification of hardware problems at the earliest possible stages. This will allow to implement necessary design modifications and reduce the risk for the flight model performance.

Alternative Model Philosophy and Schedule

In order to meet the NASA need dates for the NGST instruments, the above presented „standard“ schedule has to be reduced in time. This will lead to a reduction of models and a corresponding increase of risk.

Besides technology breadboards and prototypes, the following models are proposed:

- Structural/Thermal Model (STM)
- Optical Engineering Model (OEM)
- Proto-Flight Model (PFM)
- Flight Spare

The alternative model philosophy is shown in Figure 2.3-3 below.

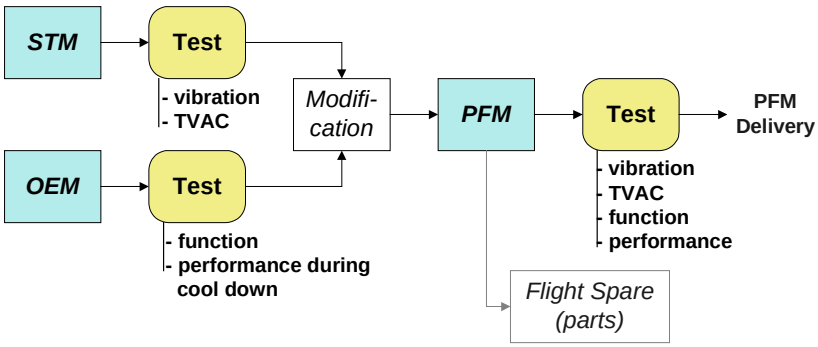

Figure 2.3-3: Alternative (NASA compatible) Model Philosophy

Even with a reduced development program the STM is still considered mandatory to test the performance of the large instrument structure at low operating temperatures and after launch loads. Necessary design modifications are likely and will be derived for the PFM. After testing, the STM will be shipped to NASA for system level tests.

In parallel to the STM, an OEM will be equipped such that an opto-mechanical (and electrical) verification of the concept can be performed at ambient temperature and at moderately lowered temperatures. The OEM will undergo an accelerated performance and environmental test program. It cannot be expected that the OEM will provide satisfying performance at operational temperature, but its behavior during cool-down, together with the STM test results, will provide valuable inputs for PFM improvements.

The PFM will be the first instrument model to be fully tested at acceptance levels. The flight spare will consist of a set of instrument functional units and spare parts.

Major drawbacks of this approach are:

- the final impacts of the structural/ thermal and opto-mechanical modifications can not be clarified before PFM availability
- the first real optical verification of the instrument will be performed on the flight model

Although with this alternative approach the associated risk is higher than for the standard model philosophy, it nevertheless bears the potential to meet the requested NASA need dates.

2.3.3 Schedule

The development schedule for both the standard and the NASA compatible approach are shown in Figure 2.3-4.

Up to and including Phase B the schedules are identical. However, the short PFM delivery date of the NASA compatible approach has repercussions not only on the shorter procurements phase but also on previous phases. In this case the technology readiness should be ensured at the beginning of Phase B and all manufacturing files should be finished at PDR (end of Phases B) in order to allow immediate start of hardware realization at the beginning of Phase C/D.

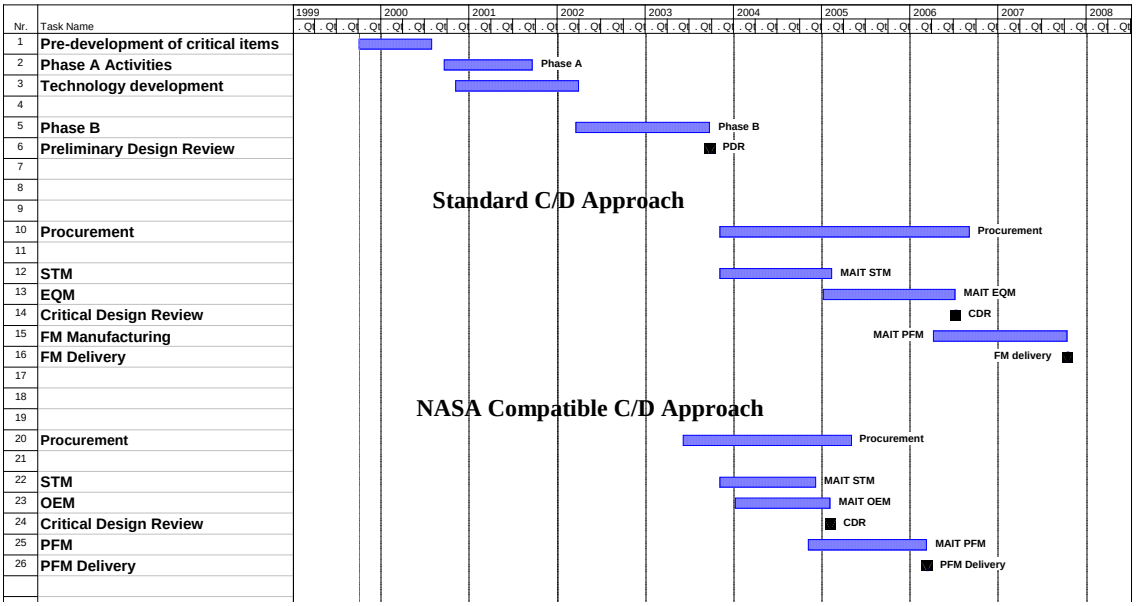

Figure 2.3-4: Proposed development schedule for both model philosophies

3 MIRIFS ENGINEERING

Note: details on mechanical, thermal and electrical design can be found in ref. /3/.

3.1 MIRIFS Design Concept

3.1.1 General Optical Design Considerations

The instrument consists of three subsections: fore-optics and image slicers, SW spectrograph and LW spectrograph.

The fore-optics are used to divide the optical beam from the telescope into two wavelength channels and to re-image the telescope focal plane onto the slicing mirrors.

The image slicer design is based on the design developed at the UK-ATC (Astronomy Technology Centre) for the Imager Spectrometer, UIST, which is under construction for the United Kingdom Infrared Telescope. This slicer already had sufficient slices to meet the MIRIFS field requirement for the pixel scales above. An existing image slicer design was chosen to reduce the risk and unknown factors in the design of MIRIFS. The detailed opto-mechanical design of this slicer was driven by the need to ensure that the device could be manufactured by conventional means and tested as individual components and as sub-assemblies, and to minimise the number of optical elements used. The optical surfaces are either spherical or flat, to simplify the testing of the components. The magnification of the image is chosen so that the individual slicing mirrors are 1mm thick, to ensure that the mirror substrates remain flat after manufacture.

It was decided to split into the two channels at a wavelength of 10µm, because this minimises the effect of the thermal backgrounds from the instrument optics on the short wavelength sensitivity. Since the detectors are sensitive to wavelengths out to 28µm any red-leaks in the filters would have a serious impact (see also discussions in /3/). A dichroic beamsplitter therefore reflects the 10 - 28µm band.

In the early stage of design both reflective and refractive designs for the spectrographs and dispersing elements were considered. In principal the refractive designs may be more compact, but the control of thermal background and achromaticity are significantly better for all-reflective designs. In addition, for wavelengths longer than 18µm the only refractive material is KRS5. Although KRS5 grisms have been manufactured, and KRS5 was used in ISO it is a dense and weak material for which there are problems and risks in mounting the relatively large pieces that would be required. For all of these reasons an all-reflective design was chosen for both channels.

3.1.2 *Fore-Optics and Image Slicer Design Description*

The optical layout of the fore optics and image slicer are shown in Figure 3.1-1 below:

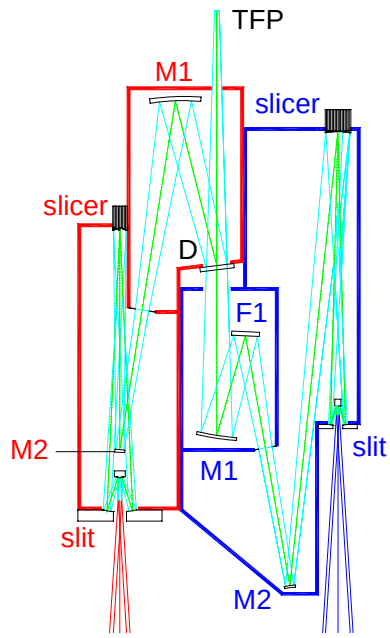

Figure 3.1-1: Optical Configuration for the fore-optics and image slicers. The short-wavelength (5-10µm) channel is outlined in blue, long wavelength (10-28µm) in red.

The telescope focal plane, TFP, is a short distance from the instrument envelope. The dichroic beamsplitter, D, reflects the light for the LW channel (shown in red) and transmits that for the SW channel (shown in blue). A substrate of ZnSe is proposed for the dichroic, which is the first optical element so that the two channels of the spectrograph can be assembled and tested independently.

Toroidal mirrors, M1 and M2, re-image the f/16 telescope focal plane, TFP, on to the two slicing mirrors. Toroidal mirrors are needed to provide sufficiently good image quality at the slicing mirrors.

M1 produces an intermediate pupil which is necessary to control stray light by a stop placed in a baffle which separates the fore-optics from the image slicer. The fold mirror, F1, gives the reflection necessary to direct the output from the SW slicer downwards towards the spectrograph. The long axis of the slits is into the paper in this view and the length of the LW slit sets the overall depth of the fore-optics module.

The illustration in Figure 3.1-2 shows the fore-optics and image slicers. The dichroic beamsplitter separates the two channels by wavelength and the mirrors M1 and M2 re-image the telescope focal plane, greatly magnified, on the arrays of slicing mirrors.

The slicing mirrors are 1mm broad, 28mm high and each has a concave spherical surface. These act as reflective slits splitting the focal plane and directing the light into two groups of output beams. Four of the beams are illustrated here in red, blue, green and magenta. The slicing mirrors produce a real pupil in each beam. These pupils form two rows and masks at these pupil planes are used to control stray light.

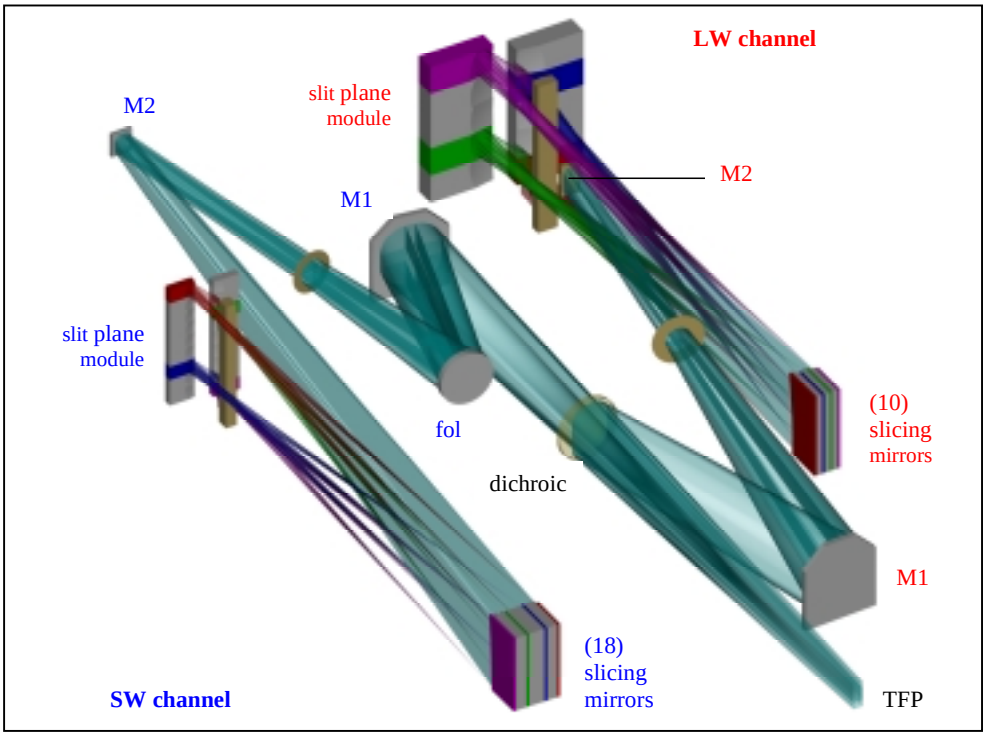

Figure 3.1-2: Scale illustration of fore-optics and the two image slicers, showing the beam path. The short wavelength channel has 18 slicing mirrors, while the long wavelength has 10.

Note that the output from the slicing mirror is not only spread vertically to separate the slit images, but also laterally so that the pupils form two rows, which means that the re-imaging mirrors have a lateral symmetry and can be made as two sets of nine (five) mirrors rather than as one set of eighteen (ten) different mirrors. The image slicers are anamorphic in the sense that the width of each slice, and hence the spatial sampling in the dispersion direction, is 2-pixels, but the spatial sampling along the slice is 1 pixel. (This is the equivalent of having a 2-pixel wide slit in a long-slit spectrograph).

The separated beams are re-imaged by individual concave mirrors to form images of the slices in two parallel rows, 2.5mm apart. The slices in each row have a gap between them which is slightly larger than the height of a slice and the two rows are offset so that a slice in one row locates in the gap in the other row. A central roof mirror diverts the slit images so that they appear at the entrance to the spectrograph as a long, staggered, slit as shown in Figure 3.1-3.

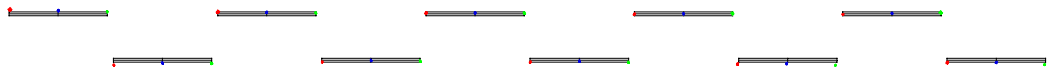

Figure 3.1-3: The staggered slit of the 10 slice LW channel

The magnified view of Figure 3.1-4 shows the slit plane module of the LW channel. This consists of the 10 re-imaging mirrors and a long roof mirror. The real pupil formed by the slicing mirrors is clearly visible in the individual beams, as is the slit image formed after the roof mirror. The re-imaging of the pupil produced by the image slicer is combined with the re-imaging of the slit, thereby avoiding the need for a powered optical component at the output slit plane, and reducing the number of powered components by a third.

A mask at the pupil plane, not shown, is used to prevent stray light from passing onwards into the spectrograph. The apertures in it will need to be sized for a specific wavelength and will vignette the beam at longer wavelengths. A Dekker mask at the slit plane, also not shown, limits the slit image in the spatial direction and thus sets the number of pixels which are left un-illuminated between each spectrum. The spectrometer slit is defined by the slicing mirrors and in the dispersion direction this Dekker mask is sized to transmit all of the light in the reimaged TFP.

A similar layout is used in the SW channel, but with 18 re-imaging mirrors. A close up view, this time including the pupil mask to control scattered light and thermal background, and the mask at the slit plane is shown in Figure 3.1-5 below.

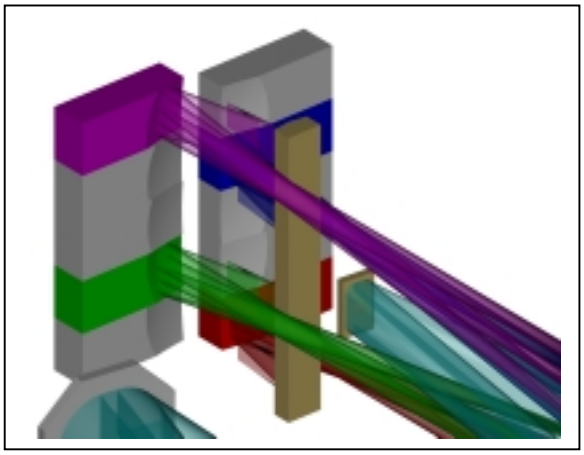

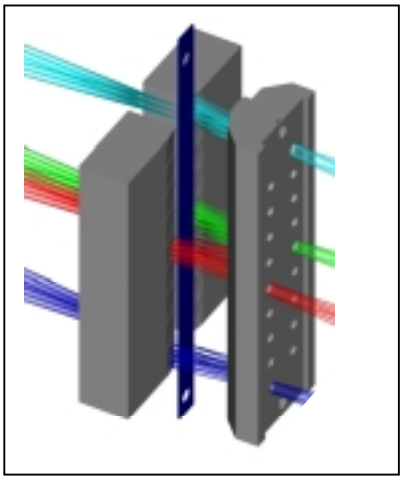

Figure 3.1-4 (left): Magnified view of the slit plane module for the long wavelength channel

Figure 3.1-5 (right): Magnified view of the slit plane module for the short wavelength channel

3.1.3 Short Wavelength Channel

The entrance aperture to the short wavelength (SW) spectrograph is the slit mask of the SW image slicer, which is shown in the upper left of Figure 3.1-6.

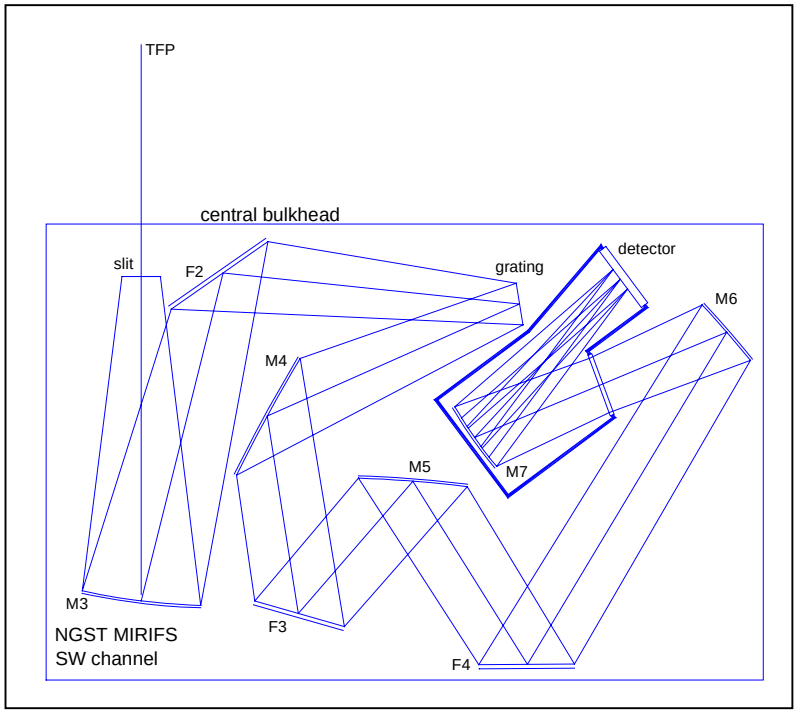

Figure 3.1-6: SW Spectrometer Optical design

The SW spectrometer is designed to fit on one side of a central rectangular plate which supports, and separates, the two channels. Note that the long axis of the slit is now shown in the plane of the paper *i.e.* this view is a side view, the view of the fore-optics in Figure 3.1-1 was a front view.

The collimator is a single mirror, M3, which produces a 50mm pupil at the grating. A fold mirror, F2, makes the collimator section more compact. The grating has a fixed incidence and is used in semi-Littrow mode. The ruling spacing is 28 lines per mm and the blaze angle is 13.85 degrees.

The camera consists of four toroidal mirrors; M4, M5, M6 and M7. They produce a tilted focal plane at the detector and an intermediate pupil, between M6 and M7. A blocking filter is placed at the pupil to limit background loading on the detector. The tilt of this filter re-directs the rejected light in such a way that it can be effectively trapped. The detector is mounted on a printed-circuit board which acts as its support structure. Two fold mirrors, F3 and F4, are needed to fit the camera section into the space envelope. Table 3.1-1 summarizes the design parameters for the SW spectrograph design and the SW fore-optics and image slicer.

Parameters of MIRIFS - SW	
Parameter	**Value**
Wavelength Range	5 to 10µm
Field of view	5.4 x 8.5 arcsec^2
Plate Scale	0.15 arcsec/pixel
Spectral Resolution (Nyquist sampled)	R=1000 at 5µm R=2000 at 10µm
Number of slices	18
Filters	1 fixed order sorting and long wave blocking filter
Detector Array size	2K (spectral) x 1 K (spatial)
Detector Pixel Size	27µm
F-number at Object side	16
Entrance pupil	telecentric
Intermediate Pupil stops	in re-imaging optics and in image slicers
Cold Stop	at filter
Filter Diameter	90 mm
F-number at slicing mirrors	86
Collimated beam diameter in spectrograph	50 mm
Grating	28 l/mm rule , blaze 13.85 degrees
Spectrograph camera F-number	4.64

Table 3.1-1: MIRIFS–SW design parameters

3.1.4 Performance of the SW Channel

The fore-optics image quality ensures that 100% of the energy falls within one slice width for all wavelengths and positions in the field. The simple optics in the image slicer do of course introduce aberrations and these are passed to the spectrograph.

The following discussion covers the performance of the entire SW channel: fore-optics + image slicer + spectrograph. In Figure 3.1-7 we show a graph of the average Strehl ratio for each slice, for wavelengths that are at the edges and center of the spectrograph field. The image quality varies along the slice, being better on-axis, near the center of the slice, than at the ends, and the average is used here as a representative value. The actual values for the Strehl ratio are given in the table underneath the graph.

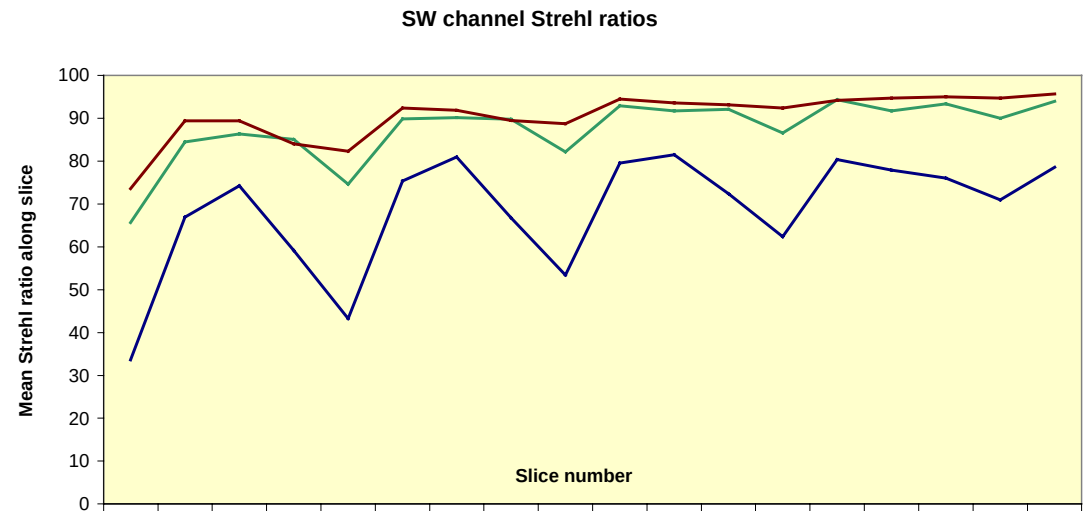

	1	2	3	4	5	6	7	8	9	10	11	12	13	14	15	16	17	18
λ=5	34	67	74	59	43	75	81	67	53	80	81	72	62	80	78	76	71	79
λ=7.5	66	84	86	85	75	90	90	90	82	93	92	92	87	94	92	93	90	94
λ=10	74	89	89	84	82	92	92	89	89	95	94	93	92	94	95	95	95	96

Figure 3.1-7: Strehl ratios for the SW channel

The blue line on the graph shows that at 5µm the overall performance is not close to diffraction limited for slices 1,5,9,13. These slices are furthest from the axis of the spectrograph and so at 5µm are at the extreme edge of the field.

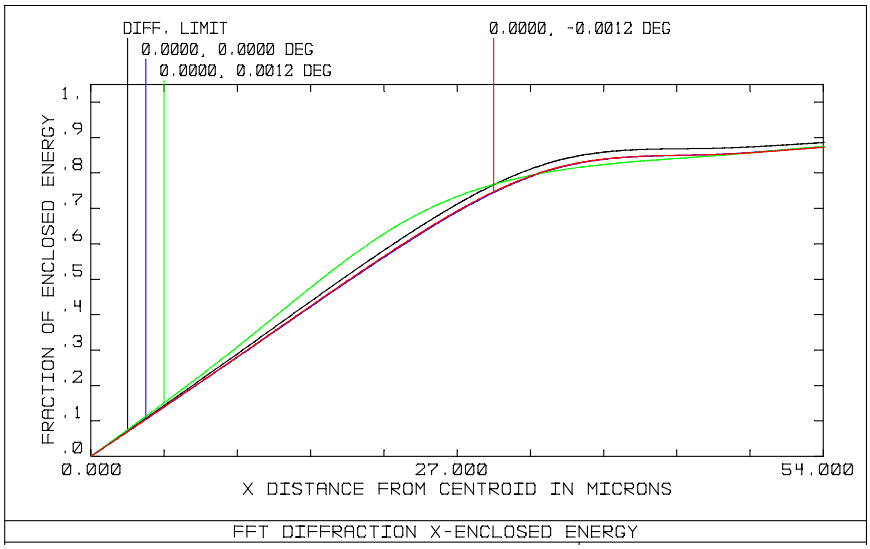

Figure 3.1-8: Enclosed energy plot of typical SW slice, calculated at 7.5 µm

Since the pixel size of 0.15arcsec critically samples the full width half maximum of the diffraction limit at 10µm, at the shorter wavelengths it is larger than the diffraction limited spot, and so a low Strehl ratio is not necessarily a problem. It is

more important that the light falls within the 2-pixels per resolution element so that spectral resolution is not degraded. In Figure 3.1-8 we show the diffraction broadened enclosed energy found by integrating the image in the spatial direction. The x-axis is the half-width of the integration limits so that the graphs show the integral out to limits of 2 pixels.

3.1.5 Long Wavelength Channel

A similar concept is used for the long wavelength channel, but since fewer spectral pixels are available to cover a wider wavelength range, 3 orders of the grating are used. Since the plate scale is larger and the total field of view was a limiting factor in the spectrograph design, fewer slices were used in the image slicer. The optical layout is shown in Figure 3.1-9 below

The LW spectrometer optics are designed to mount on the other side of the plate from the SW spectrometer. In this view, the slit produced by the fore-optics is shown at upper right. As can be seen, the overall extent of the central bulkhead is set by the SW spectrograph, and there is more free space around the optics.

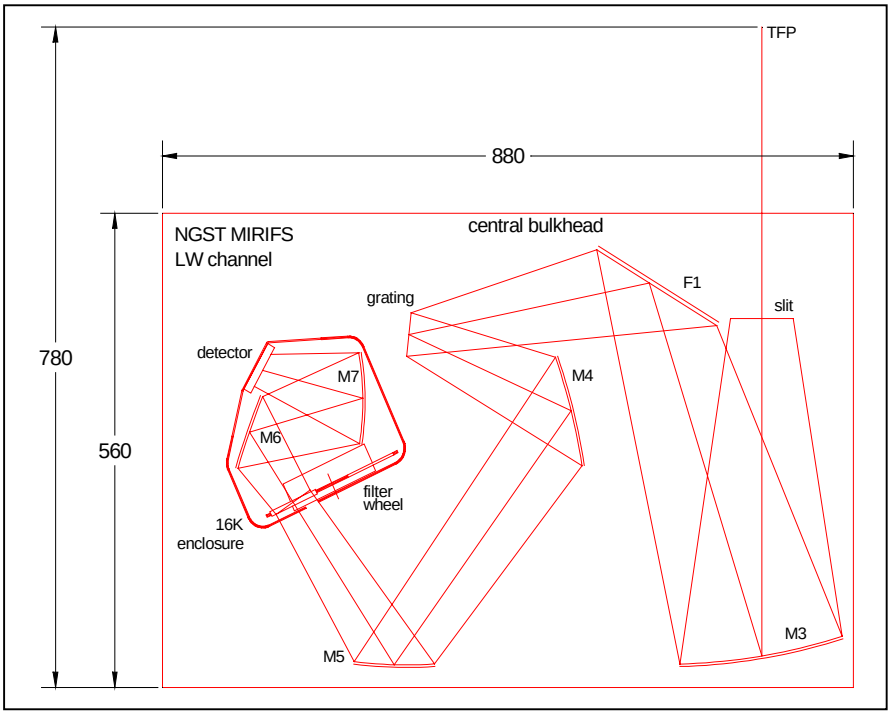

Figure 3.1-9: Long Wavelength optical layout

The collimator is a single mirror, M3, which produces a 50mm diameter pupil at the grating. A single fold mirror, F1, makes this channel more compact. The grating has a fixed incidence and is used in semi-Littrow mode. The ruling spacing is 8.08 lines per mm and the blaze angle is 12.24 degrees.

The camera consists of four toroidal mirrors; M4, M5, M6 and M7. They produce a tilted focal plane at the detector and an intermediate pupil. A filter wheel, the only mechanism in MIRIFS, puts one of three order-sorting filters into the beam at the pupil and also has a clear hole. The wheel can be based on one of the ISO mechanism designs. The tilt of the filter re-directs the rejected light in such a way that it can be effectively trapped. The detector, filter wheel and mirrors M6 and M7 are enclosed in a box which is cooled to 18K to control background.

Table 3.1-2 summarizes the design parameters for the LW spectrograph design and includes the LW fore-optics and image slicer.

Parameters of MIRIFS - LW	
Parameter	**Value**
Wavelength Range	10 to 30 µm
Field of view	6 x 10 arcsec^2
Plate Scale	0.3 arcsec/pixel
Spectral Resolution (Nyquist sampled)	R = 1000 at 10µm to R = 2000 at 20µm
Number of slices	10
Filters	3 selectable order sorting filters
Detector Array size	1K (spectral) x 1 K (Spatial)
Detector Pixel Size	27µm
F-number at Object side	16
Entrance pupil	telecentric
Intermediate Pupil stops	in re-imaging optics and in image slicers
Cold Stop	at filter
Filter Diameter	55 mm
F-number at slicing mirrors	43
Collimated beam diameter in spectrograph	50mm
Grating	28 l/mm rule , blaze 13.85 degrees
Order 4 wavelength range and resolution	10 - 15µm, R = 1000 - 1500
Order 3 wavelength range and resolution	15 - 20µm, R = 1500 - 2000
Order 2 wavelength range and resolution	20 - 30µm, R = 1000 - 1500
Spectrograph camera F-number	2.32

Table 3.1-2: MIRIFS-LW design parameters

3.1.6 Performance of the LW Channel

The following discussion covers the performance of the entire LW channel: fore-optics + image slicer + spectrograph. In Figure 3.1-10 we show a graph of the average Strehl ratio for each slice, for wavelengths that are at the edges and center of the spectrograph field. The image quality varies along the slice, being better on-axis, near the center of the slice, than at the ends, and the average is used here as a representative value. The actual values for the Strehl ratio are given in the tables underneath the graphs.

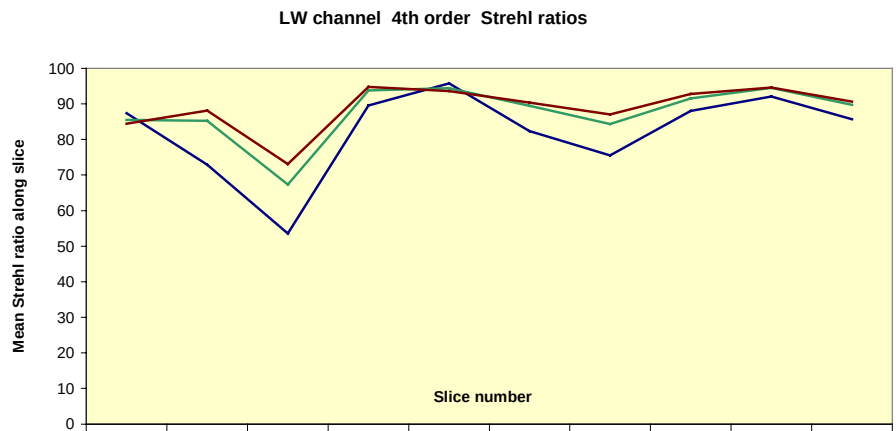

	1	2	3	4	5	6	7	8	9	10
λ=10	87	73	54	90	96	82	76	88	92	86
λ=12.5	86	85	67	94	94	89	84	92	94	90
λ=15	84	88	73	95	94	90	87	93	95	91

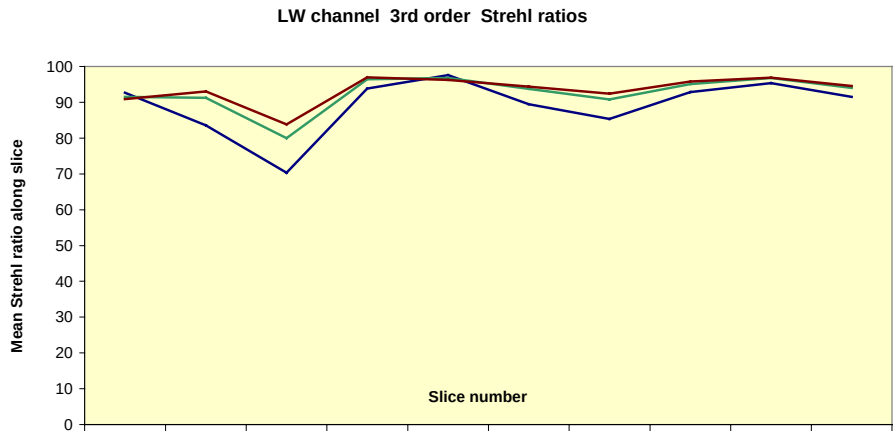

	1	2	3	4	5	6	7	8	9	10
λ=13.3	93	84	70	94	98	89	85	93	95	92
λ=16.7	92	91	80	96	97	94	91	95	97	94
λ=20	91	93	84	97	96	94	92	96	97	95

Figure 3.1-10: Average Strehl ratios as a function of slice number and wavelength

The graphs show the Strehl ratio for orders 3 and 4 only, that for 2nd order has the same form as that for order 4, but the values are all >> 80% because the wavelengths are longer. Except for slice 3 at 10µm the performance is very good, and for slice 3 it is acceptable in the sense that 70% of the encircled energy falls within one resolution element. Figure 3.1-11 shows an enclosed energy plot at 12.5 µm.

The performance of slice 3 could be improved by a small further optimization of the fore-optics/slicer combination.

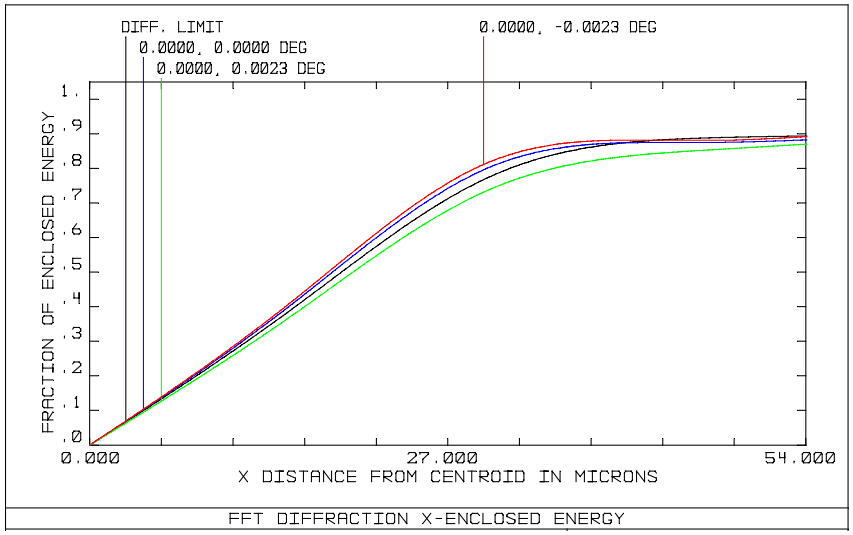

Figure 3.1-11: Encircled energy for LW slice, calculated at 12.5 µm

Throughput

The overall transmission of the spectrometers is given in Table 3.1-3. These calculations are based on the reflectivities and expected transmissions of the optical components. There will be diffraction effects, especially at the long end of each wavelength range; a detailed study of these effects needs to be done in the next phase.

Component	Throughput
Mirrors	85%
Filter and dichroic	80%
Grating	80%
Total	54%

Table 3.1-3: Optics transmission

3.1.7 Instrument Photometric Performance

A photometric performance model has been established to simulate the expected in-orbit instrument performance. The model includes all efficiencies from the telescope transmission up to the detector quantum efficiency. As photon background the following contributions have been considered

- zodiacal light (ref. /4/)
- emission from sunshield, scattered by telescope prime mirror (ref. /5/)
- emissions from warm optics in front of the filter
- emissions from cold optics and walls up to and including the filter

Figure 3.1-12 shows the detectable flux [µJy] of point objects as a function of wavelength that can be resolved with the integral field spectrograph in the short and the long wavelength region with a SNR of 10 and for 10^5 sec observation time.

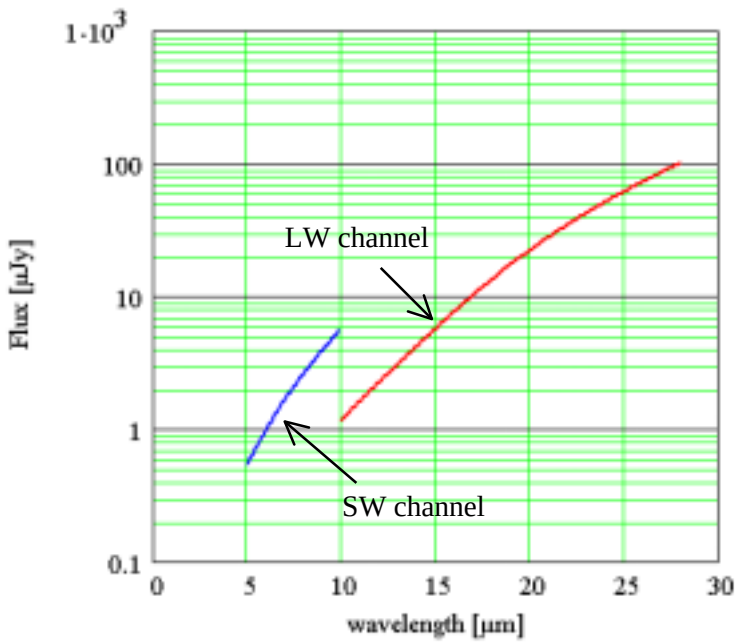

Figure 3.1-12: detectable flux [µJy] of point sources vs. wavelength that can be resolved in the short and long wavelength region with an SNR of 10 for an observation time of 10^5 sec. The average resolution is R ~ 1500.

Discussion of Result

At wavelengths < 12 µm and faint objects the performance is detector noise limited. In order to improve the performance at those wavelengths the detector dark current should ideally be an order of magnitude lower (at 5 µm it should ideally reach the performance of the NIR detectors). The big step between SW and LW channel is due

to the change of resolution. The theoretical factor 4 is increased further by detector noise, which is relatively more critical in SW than in LW channel.

At wavelengths above 12 µm the performance is photon noise limited. As for the MIR camera, the dominant noise sources are the zodiacal light and – much worse – the scattered light from the sunshield. If the surface quality of the telescope prime mirror cannot be improved considerably, then the scattered light contribution can only be reduced by lowering the sunshield temperature from 90 K to about 70 K.

In case the ISIM is at < 35 K the emissions from the warm optics are negligible. The cold optics temperature of < 18 K has been selected such that this contribution will also be negligible. Assuming Fowler sampling the readout noise is negligible in all cases.

3.1.8 Opto-Mechanical Design

The baseline opto-mechanical designs are shown in Figure 3.1-13 to Figure 3.1-17.

The optical bench as primary structure consists of a light-weighted plate made of C/SiC material. The C/SiC brackets for the optical components are directly attached to the baseplate. The mirrors are connected to the brackets by an isostatic 3 point support. Flexible INVAR mounts are used as connection elements.

In Figure 3.1-14 and Figure 3.1-15 the cold housing cover is removed to show the accommodation of the cold optical elements inside.

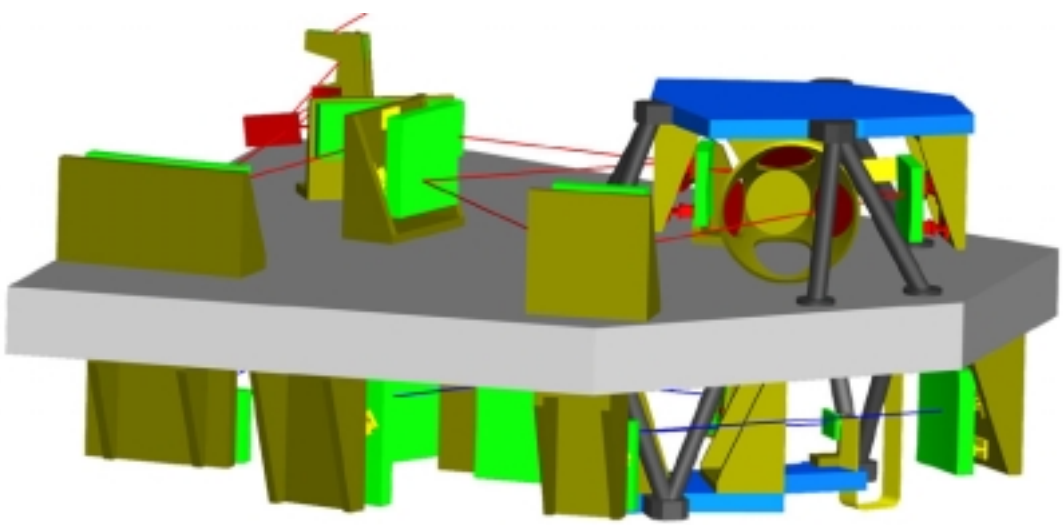

Figure 3.1-13: MIRIFS design: 3D view of overall instrument (upper part is LW channel)

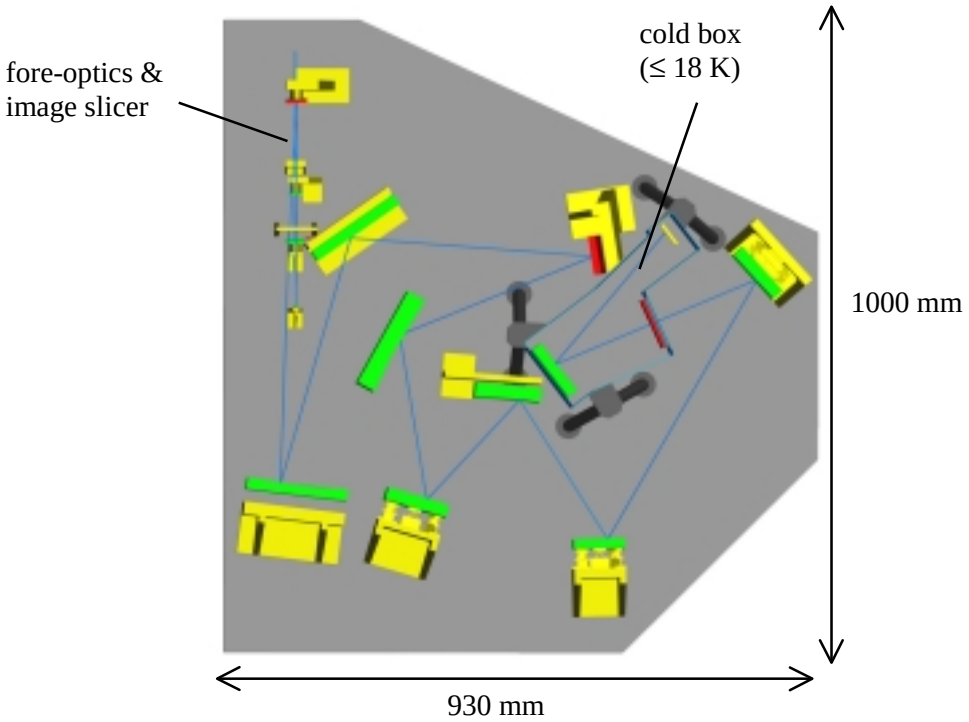

Figure 3.1-14: MIRIFS opto-mechanical design of SW channel

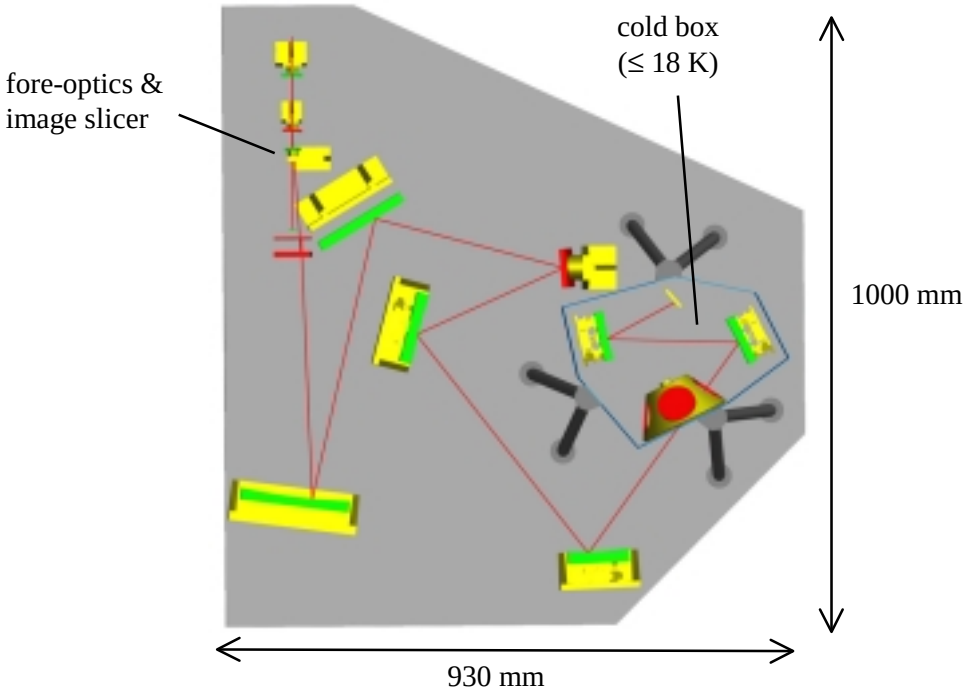

Figure 3.1-15: MIRIFS opto-mechanical design of LW channel

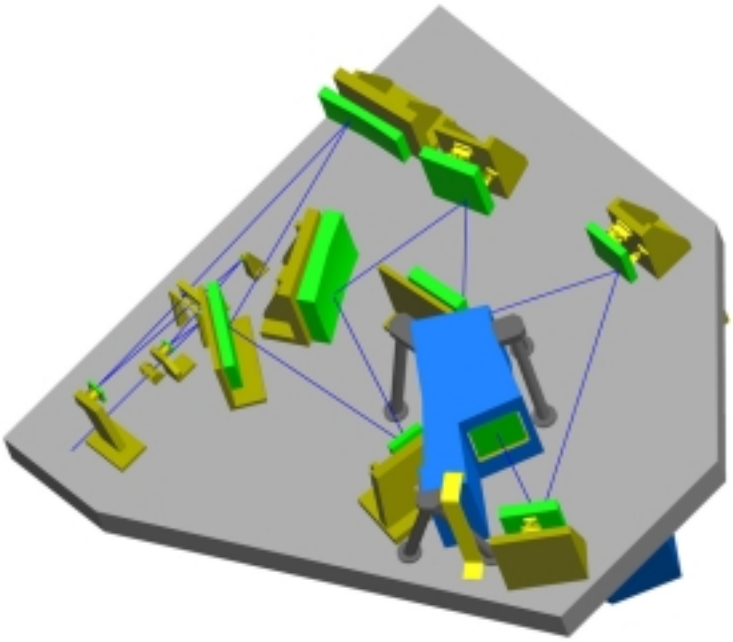

Figure 3.1-16: MIRIFS design: 3D view of SW channel

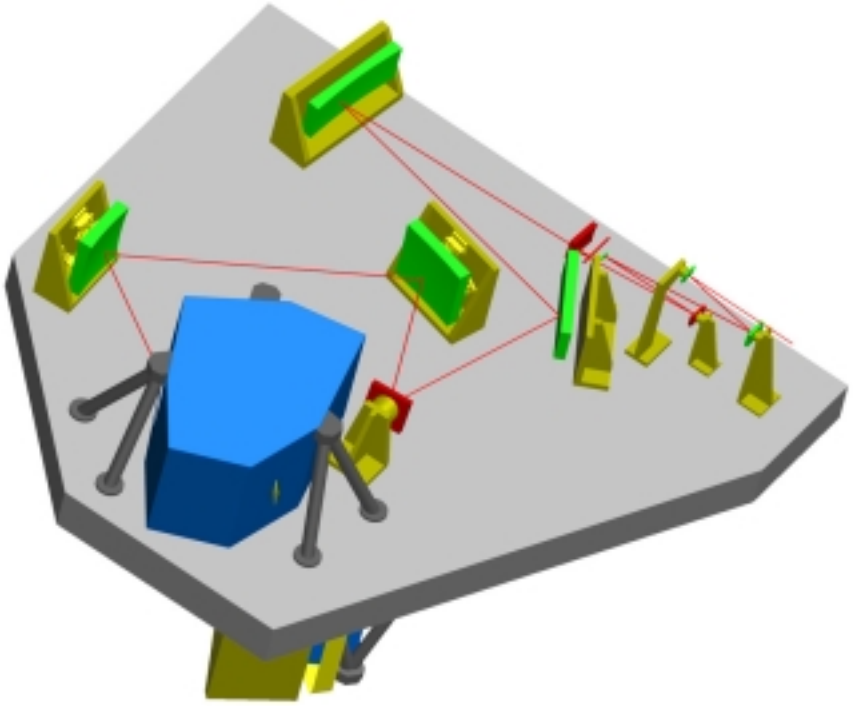

Figure 3.1-17: MIRIFS design: 3D view of LW channel

3.1.9 Budgets

The overall dimensions are: 1.00 x 0.93 x 0.44 m^3

The estimated overall mass of the MIR spectrograph is 55 kg (Table 3.1-4).

	Mass [kg]
Primary structure	36
Brackets, mounts, filter wheel	3.5
Optical components	5
Thermal hardware	0.5
Miscellaneous (I/F brackets, harness, etc.)	10
Total	**55**

Table 3.1-4: MIRSPEC mass budget

3.1.10 Conclusions

The instrument is quite compact given the fields of the IFUs which are equivalent to a ~ 100 arcsec long slit. Lower spectral resolution would result in a smaller instrument, and might remove the need for a filter wheel in the LW channel.

Summary of features:

+ very good image quality for the LW-range, adequate for the SW
+ compact, simple image slicer design.
+ pupil location in slicer can be used for baffling - important for control of background and scattered light at these long wavelengths.
+ good cold stop located after the grating for control of stray light and background.
+ thermal design guarantees a good reduction of background radiation
+ SW channel has no moving parts, and only 1 filter wheel required in LW channel.
+ two channels may be assembled and tested independently.
- all spherical image slicer optics limit the performance at 5µm

Possible Improvements:

+ better optimization of the image slicer design for the SW channel, replacing the spherical mirrors with toroids, is possible

Special studies to be done in the next phase:

- more detailed science analysis of requirements for spectral resolution.
- analysis of stray-light and thermal self-emission
- analysis of diffraction effects on throughput and image quality

3.2 Critical Areas and Recommended Development Activities

3.2.1 Instrument Hardware Breakdown

Figure 3.2-1 shows the HW breakdown of the filter wheel camera. The shaded boxes provide an overview of potential critical subsystems or of subsystems containing critical elements as listed in chapter 2.2.2.

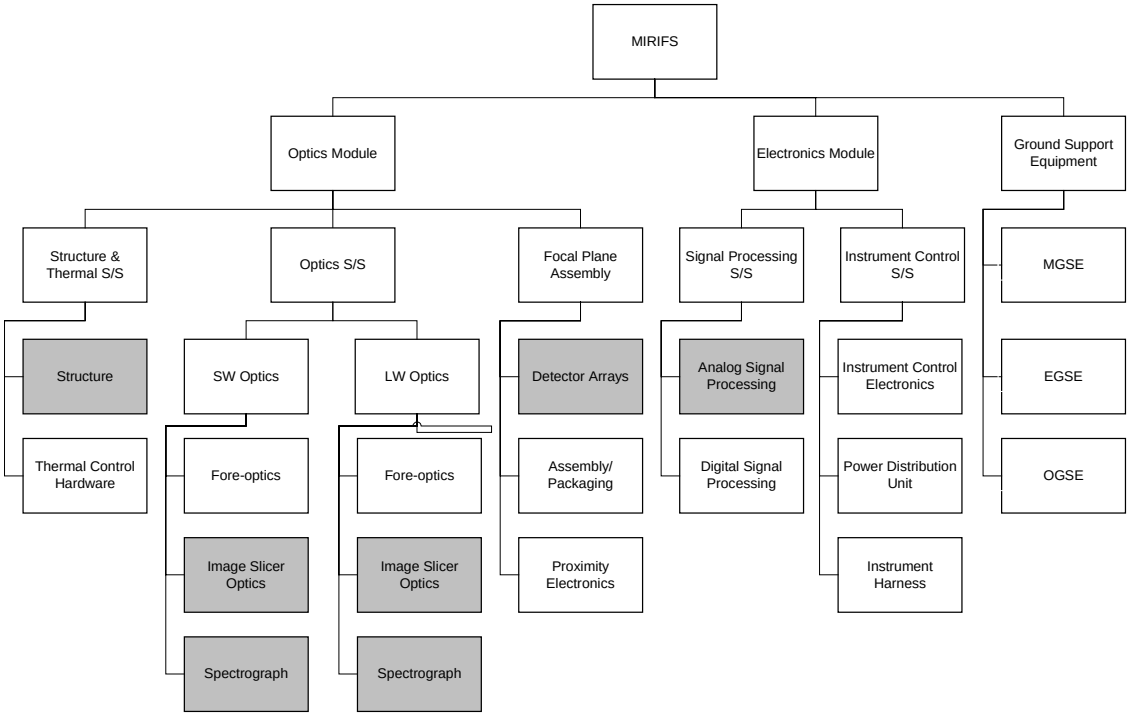

Figure 3.2-1: Instrument Hardware Breakdown; shaded areas indicate potential critical subsystems.

3.2.2 Critical Areas and Technology Requirements

The general critical areas and technology requirements are identical to the MIRCAM and will not be iterated below: reference is made to chapter 2.2.2.

Critical Areas and Risks

Instrument specific areas of potential criticality for MIRIFS are summarized in the following Table 3.2-1.

Subsystem	Critical area	Comments
image slicer	alignment at operational temperature	thermal deformations during cool-down
	suppression of straylight and optical cross-talk	diffraction effect
spectrograph	testing of toroidal mirror figure quality	requires sophisticated test equipment

Table 3.2-1: Potential critical areas of MIRIFS

Technology Requirements

The potential criticality of the image slicer unit lies within the amount of small optical parts to be assembled at ambient and kept stable during cool-down to operational temperatures. Another point of criticality may arise from the fact that due to diffraction at the edges of the slicer mirrors the beam diameter at longer wavelengths is larger than the reimaging mirrors, which may result in optical cross-talk. Therefore the image slicer performance at low temperatures should be verified by test.

The manufacture and testing of toroidal mirrors is considered of lower criticality, which may not require dedicated technology development but can be handled with careful planning of ressources.

Another point of concern is the long distance from the detector array to the analog signal processing electronics. Since the SW channel detectors are working in the detector noise limit they are especially susceptible to possible EMI. For this channel close-by preamps should be considered.

3.2.3 Recommended Follow-On Activities

Besides the general recommended technology development activities of chapter 2.2.3 and ref. /3/ the following instrument specific activity is recommended.

- verification of image slicer alignment stability and straylight suppression

For each of these activities, the following technology development activities are proposed:

- critical review of existing technologies
- design and manufacturing of a representative unit
- verification of performance prior to and after environmental tests, at ambient and at operating conditions

The expected duration of the development activities is 15 months.

Note: a similar image slicer unit for ground applications (UIST) is currently being manufactured and will undergo performance testing at temperatures down to 55K in the near future.

3.2.4 Technology Development Roadmap

The technology development roadmap for the major critical technologies is depicted in Figure 2.2-2 below.

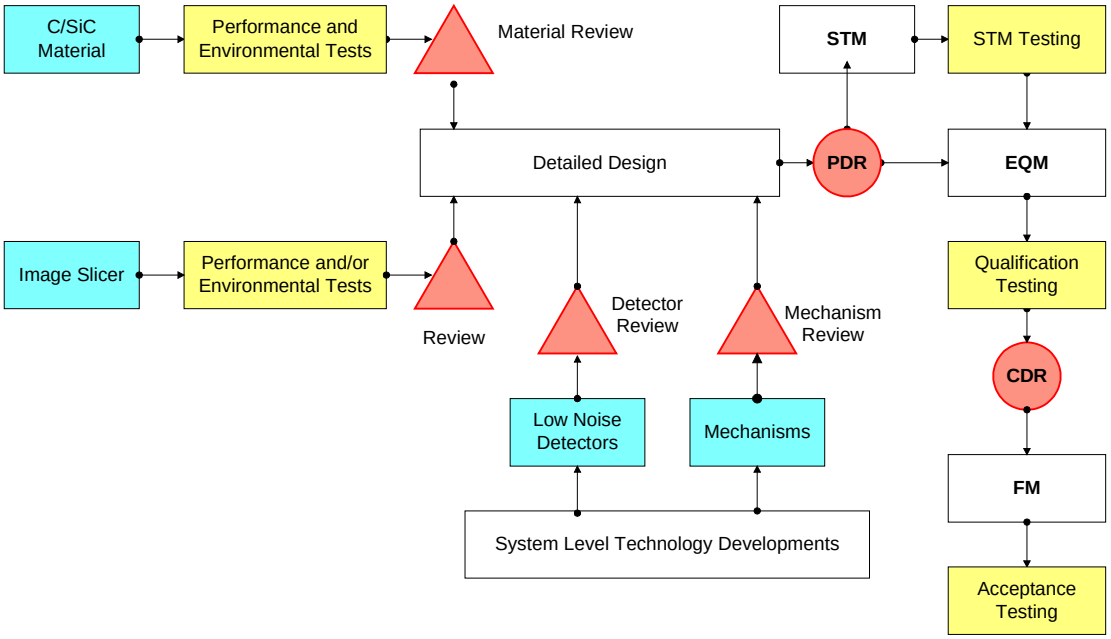

Figure 3.2-2: Technology Development Roadmap

3.3 Development Planning

The MIRIFS development planning is the same as for the MIRCAM.

Please refer to chapter 2.3.

4 REFERENCES

/1/ "Study of Payload Suite and Telescope for NGST", ESTEC/Contract no. 13111/98/NL/MS

/2/ Statement of Work for "Study of Payload Suite and Telescope for NGST", PF-NGST-SOW-002, Issue 1, 24-Apr-98

/3/ "NGST Payload Study, General Design Considerations", NGST-DSS-WHRP-001, 01-Oct-99

/4/ NASA Exposure Time Calculator

/5/ "Implications of the Mid-Infrared Capability for NGST", P. Bély et.al., 9-Nov-98, chapter 2.1